JOURNAL OF PETROLOGY | VOLUME 55 | NUMBER 4 | PAGES 803–830 | 2014 | doi:10.1093/petrology/egu007

Dating Polygenetic Metamorphic Assemblages along a Transect across the Western Alps

IGOR M. VILLA[1,2*], STEFAN BUCHER[3,4], ROMAIN BOUSQUET[3†], ILKA C. KLEINHANNS[1‡] AND STEFAN M. SCHMID[3§]

[1]INSTITUT FÜR GEOLOGIE, UNIVERSITÄT BERN, BALTZERSTR. 3, CH-3012 BERN, SWITZERLAND

[2]CENTRO UNIVERSITARIO DATAZIONI E ARCHEOMETRIA, UNIVERSITÀ DI MILANO BICOCCA, 20126 MILANO, ITALY

[3]GEOLOGISCH-PALÄONTOLOGISCHES INSTITUT, UNIVERSITY OF BASEL, BERNOULLISTR. 32, CH-4056 BASEL, SWITZERLAND

[4]RUE FONTAINE-ANDRÉ 5, 2000 NEUCHÂTEL, SWITZERLAND

RECEIVED MARCH 29, 2012; ACCEPTED JANUARY 31, 2014

Multichronometric analyses were performed on samples from a transect in the French–Italian Western Alps crossing nappes derived from the Briançonnais terrane and the Piemonte–Liguria Ocean, in an endeavour to date both high-pressure (HP) metamorphism and retrogression history. Twelve samples of white mica were analysed by ^{39}Ar–^{40}Ar stepwise heating, complemented by two samples from the Monte Rosa nappe 100 km to the NE and also attributed to the Briançonnais terrane. One Sm–Nd and three Lu–Hf garnet ages from eclogites were also obtained. White mica ages decrease from c. *300 Ma in the westernmost samples (Zone Houillère), reaching* c. *300°C during Alpine metamorphism, to <48 Ma in the internal units to the east, which reached* c. *500°C during the Alpine orogeny. The spatial pattern of Eocene K–Ar ages demonstrates that Si-rich HP white mica records the age of crystallization at 47–48 Ma and retains Ar at temperatures of around 500°C. Paleocene–early Eocene Lu–Hf and Sm–Nd ages, recording prograde garnet growth before the HP peak, confirm eclogitization in Eocene times. Petrological and microstructural features reveal important mineralogical differences along the transect. All samples contain mixtures of detrital, syn-D_1 and syn-D_2 mica, and retrogression phases (D_3) in greatly varying proportions according to local variations in the evolution of pressure–temperature–fluid activity–deformation (*P–T–a–D*) conditions. Samples from the Zone Houillère mostly contain detrital mica. The abundance of white mica with Si > 6·45 atoms per formula unit increases eastward. Across the whole traverse, phengitic mica grown during HP metamorphism defines the D_1 foliation. Syn-D_2 mica is more Si-poor and associated with nappe stacking, exhumation, and hydrous retrogression under greenschist-facies conditions. Syn-D_1 phengite is very often corroded, overgrown by, or intergrown with, syn-D_2 muscovite. Most importantly, syn-D_2 recrystallization is not limited to S_2 schistosity domains; micrometre-scale chemical fingerprinting reveals muscovite pseudomorphs after phengite crystals, which could be mistaken for syn-D_1 mica based on microstructural arguments alone. The Cl/K ratio in white mica is a useful discriminator, as D_2 retrogression was associated with a less saline fluid than eclogitization. As petrology exerts the main control on the isotope record, constraining the petrological and microstructural framework is necessary to correctly interpret the geochronological data, described in both the present study and the literature. Our approach, which ties geochronology to detailed geochemical, petrological and microstructural investigations, identifies 47–48 Ma as the age of HP formation of syn-D_1 mica along the studied transect and in the Monte Rosa area. Cretaceous apparent mica ages, which were proposed to date eclogitization by earlier studies based on conventional 'thermochronology', are due to Ar inheritance in incompletely recrystallized detrital mica grains. The inferred age of the probably locally diachronous, greenschist-facies, low-Si, syn-D_2 mica ranges from 39 to 43 Ma. Coexistence of D_1 and D_2 ages, and the constancy of non-reset D_1 ages along the entire transect, provides strong evidence that the D_1 white mica ages closely approximate formation ages. Volume diffusion of Ar in white mica (activation energy* $E = 250\ kJ\ mol^{-1}$*; pressure-adjusted diffusion coefficient* $D'_0 < 0{\cdot}03\ cm^2\ s^{-1}$*) has a subordinate effect on mineral ages compared with both prograde and retrograde recrystallization in most samples.*

*Corresponding author: Telephone: +41 31 631 8777. Fax +41 31 631 4843. E-mail: igor@geo.unibe.ch

†Present address: Institut für Geowissenschaften, Christian-Albrechts-Universität, 24118 Kiel, Germany.

‡Present address: FB Geowissenschaften, Eberhard-Karls-Universität, Wilhelmstraße 56, 72074 Tübingen, Germany.

§Present address: Institut für Geophysik der ETH, Sonneggstrasse 5, 8092 Zürich, Switzerland.

KEY WORDS: *^{39}Ar–^{40}Ar geochronology; Ar diffusion; eclogite dating; retrograde reaction dating; Western Alps*

INTRODUCTION

Quantifying rates of processes during the evolution of orogens requires direct time constraints. However, providing ages for phases of deformation in basement–cover assemblies that have undergone polyphase metamorphism is challenging [see review by Vance *et al.* (2003) and references therein]. High spatial resolution *in situ* dating techniques, such as U–Pb age mapping of zircon grains by ion microprobe and of monazite grains by electron microprobe, and U–Pb and ^{39}Ar–^{40}Ar age mapping by laser ablation, complement the well-known petrographic observation that different populations of grains are often present within the same thin section by documenting multimodal age distributions even at the micrometre scale (Villa & Williams, 2013, and references therein). However, *in situ* dating techniques have their limitations, especially in young metamorphic terrains such as the Alps (Müller *et al.*, 2002) because precision is limited by low concentrations of radiogenic isotopes.

The ^{39}Ar–^{40}Ar stepwise heating technique is preferred for dating polygenetic white mica samples because it provides a control on the chemical composition of the degassed Ar reservoirs (Rex *et al.*, 1993; Villa *et al.*, 1997, 2000; Müller, 2003; Vance *et al.*, 2003); that is, of the identity of the different phases or mineral generations in a sample. This is based on the ^{37}Ar/^{39}Ar ratio (Wartho, 1995), or the combination of ^{38}Ar/^{39}Ar and ^{37}Ar/^{39}Ar ratios (Villa *et al.*, 1996, 2000; Belluso *et al.*, 2000), which reflect the Ca/K and Cl/K ratios. The *in situ* ^{39}Ar–^{40}Ar laser probe technique cannot be exploited for these samples, despite its potentially high spatial resolution, as the smallest useful volume for analysis is determined by the least abundant isotope/s required for a successful analysis (Villa & Williams, 2013), which, for this study, are ^{38}Ar and ^{37}Ar. It has been shown that stepwise heating of polymineralic mixtures provides better accuracy than laser microprobe ages (Müller *et al.*, 2002), especially when the size of the metamorphic intergrowths is smaller than the effective spatial resolution of the laser ablation volume (Agard *et al.*, 2002). Incremental heating and single-spot fusions are complementary methods capable of producing consistent results (Philippot *et al.*, 2001; Müller *et al.*, 2002; Challandes *et al.*, 2003; Müller, 2003). The ^{39}Ar–^{40}Ar method also benefits from the fact that the Ar retentivity of white mica is empirically well constrained (Di Vincenzo *et al.*, 2004; Allaz *et al.*, 2011, and references therein).

For this study we have analysed rocks with complex multistage metamorphic and structural histories constrained by previous research (Bucher, 2003; Bucher *et al.*, 2003, 2004; Bucher & Bousquet, 2007), combining observations at the microscopic scale and outcrop scale, all the way up to the regional context. The main objective of this combined tectonic, petrological and isotopic study is to enhance our knowledge of the processes controlling the behaviour of various isotopic systems. Twelve of the 14 samples (Table 1) were collected along a segment of a continuous crustal-scale geological–geophysical section (ECORS-CROP seismic section across the Italian–French Western Alps; Roure *et al.*, 1996) crossing the entire

Table 1: List of analysed white mica samples

Sample	Latitude (N)	Longitude (E)	Rock type	Mineral assemblage	D_0 age	D_1 age	D_2 age	D_3 age
Arv007	45°36′34·0′	6°56′53·8″	Marble	cc, phg, (chl)		>45·4	39·5	
Bez0033	45°34′1·3″	7°1′51·0″	Gneiss	phg, par, grt, chl, qtz	>90			
Cere0033	45°40′43·1″	7°4′1·3″	Gneiss	ctd, grt, phg, par, chl, czo, qtz	>76			
Cere0035	45°40′42·9″	7°4′1·1″	Gneiss	ctd, grt, phg, par, chl, czo, qtz	>230			
Ln9939	45°36′59·3″	6°57′46·8″	Meta-arkose	phg, chl, qtz, fsp		≤45 ± 3		
Mrlk1	46°4′31″	8°3′5″	Gneissic schist	grt, bt, pl, ms, ky	>77	≤47·6 ± 0·1		
Mrlk3	46°4′31″	8°3′5″	Mylonite	grt, phg, par		48·2 ± 0·1		23–29
SBPT	45°40′23·5″	7°5′0·2″	Gneiss	ctd, grt, phg, par, chl, czo, qtz	>67			
Rdl009	45°34′11·2″	7°2′48·0″	Gneiss	phg, par, grt, chl, qtz	>160	47–50		
Rui 9958	45°40′19·9″	6°59′47·1″	Meta-arkose	phg, chl, grt, ctd, qtz	>80	>43	<38	
Rui 9978	45°42′49·4″	6°59′11·7″	Meta-arkose	phg, chl, qtz, fsp	300			
Traj005	45°36′55·6″	7°17′54·4″	Metacalcschist	cc, phg, chl		48·3 ± 0·5	39–40	
Vaud003	45°29′45″	7°7′51″	Eclogite	omp, grt, phg, par, zoi		47·6 ± 0·1		
Vga0120	45°33′22·2″	7°0′22·7″	Metaquartzite	qtz, phg, (chl)			40·3 ± 0·5	<37

The complete stepwise heating data are given in Electronic Appendix Table 2. Ages are in Ma.

Briançonnais domain (Middle Penninic nappes; Schmid & Kissling, 2000; Schmid *et al.*, 2004). Two additional samples were included from the Middle Penninic Monte Rosa nappe, some 100 km away to the NE (Keller *et al.*, 2004, 2005). Within this large area the behaviour of the K–Ar system in white mica was studied for different pressure–temperature (P–T) conditions during the peak metamorphism and subsequent retrogression; the regional context and the chemical and microstructural observations make it possible to assess empirically the importance of the various processes that control the K–Ar isotopic system.

A second objective of this study is to constrain the metamorphic and deformation history on the basis of isotopic data, and also to verify and quantify the timing of the regional geodynamic evolution of the Western Alps in a self-consistent way.

GEOLOGICAL SETTING

In the 1990s, a composite seismic transect across the Western Alps was acquired by a French–Italian consortium (the so-called ECORS-CROP profile; Roure *et al.*, 1996), to understand the deep structure of a crucial portion of the world's best-studied orogen, the Alps (e.g. Schmid *et al.*, 2004). Within our study area, located along a 30 km sector of this transect (Figs 1 and 2), four major tectonic units are distinguished (Schmid & Kissling, 2000; Schmid *et al.*, 2004). These are, from external (NW) to internal (SE): the Zone Houillère Unit, the Ruitor Unit, the Internal Unit, and the Piemonte–Liguria oceanic Unit (P–L Unit), the first three being derived from the Briançonnais paleogeographical domain (Fig. 1; Fabre, 1961; Elter, 1972; Mercier & Beaudoin, 1987; Cigolini, 1995).

The Zone Houillère is characterized by a sedimentary sequence of Early Carboniferous age (Fabre, 1961). Its lower part consists of black schists with anthracitic lenses and arkoses of Namurian–Stefanian age (Feys, 1963; Gréber, 1965); its upper part is dominated by arkoses and conglomerates, probably of Stefanian–Autunian age (Fabre, 1961). A Permo-Triassic sequence discordantly overlies the Carboniferous rocks (Ellenberger, 1958; Elter, 1960).

The Ruitor Unit dominantly consists of pre-Permian garnet micaschist and paragneiss with abundant intercalated metabasites (Baudin, 1987). It exhibits an Alpine metamorphic overprint (Caby, 1996), but some relicts of pre-Alpine metamorphism survived the Alpine cycle (Bocquet, 1974a). Its sedimentary cover is made up of a thin Permo-Triassic sequence consisting of 'Verrucano'-type conglomerates (Trümpy, 1966) at the base, followed by Early Triassic meta-arkoses, which are stratigraphically overlain by quartz-phyllites and ankerite-bearing micaschists (Ulardic, 2001; Bucher *et al.*, 2004). This sequence crops out throughout the Valgrisenche valley (Fig. 2a).

The Zona Interna of Cigolini (1995) corresponds to the Vanoise–Mont Pourri Unit of Caby (1996) and will be referred to as the 'Internal Unit' below. Northwards this Internal Unit has been correlated with the Mont Fort Unit (Gouffon, 1993). The Internal Unit is made up of a lower part, formed by paragneiss and micaschist with a polymetamorphic history (Bocquet, 1974b; Cigolini, 1995; Malusà *et al.*, 2005), and a mono-metamorphic upper part, consisting of lower Permian to Mesozoic sequences. The lower part is mainly of volcanoclastic origin (Amstuz, 1955, 1962) and is intruded by Paleozoic granitic and granodioritic bodies (e.g. the Cogne granodiorite, Bertrand *et al.*, 2000). Leucocratic gneisses define the base of the mono-metamorphic upper part. These are followed by a typical Permo-Triassic sequence consisting of conglomerates ('Verrucano'), quartzitic meta-sandstones, impure quartzites, and ankerite-bearing micaschists. The younger Mesozoic cover is preserved in only the southern part of the study area.

The P–L Unit predominantly consists of calcschists, which are interlayered with variable amounts of metabasite (Elter, 1972; Cigolini, 1995). Two types of metabasite occur: eclogites, which are retrogressed in most places, and prasinites. Some researchers have proposed a subdivision of the P–L Unit within our study area into an eclogitic ('Zermatt–Saas Fee') and a non-eclogitic ('Combin') part (Droop *et al.*, 1990; Ballèvre & Merle, 1993; Dal Piaz, 1999). However, our observations indicate that both subunits represent a mélange consisting of mafic boudins metamorphosed in eclogite or blueschist facies, embedded in a matrix of metasediments that underwent the same degree of metamorphism, whereby this mélange formed during exhumation (Bousquet, 2008).

The tectono-metamorphic evolution of the portion of the internal Western Alps imaged by the ECORS-CROP profile (Bucher, 2003; Bucher *et al.*, 2003, 2004, and references therein) consists of three phases of Alpine deformation (D_1–D_3), associated with different P–T conditions prevailing in the various units (Bucher & Bousquet, 2007; Bousquet, 2008). The D_1 structures have largely been overprinted by subsequent deformation. Occasionally, relicts of D_1 are preserved on the macroscopic and microscopic scale; for example, in eclogitic boudins from the P–L Unit surrounded by a matrix of mainly greenschist-facies calcschist. Here an S_1 foliation and syn-D_1 mineral assemblage are preserved. During this first phase of deformation, associated with subduction in the Western Alps (Fig. 2b), the P–L Unit reached eclogite-facies conditions ($P > 20$ kbar, $T > 500^\circ$C). Detailed petrological investigations (Bousquet, 2008) indicate some complexity within the long-lasting subduction history referred to as D_1 (Bucher *et al.*, 2004). The peak-P mineral assemblage consists of garnet, omphacite and glaucophane, and corresponds to an early stage of D_1. Si-rich white mica occurs in many

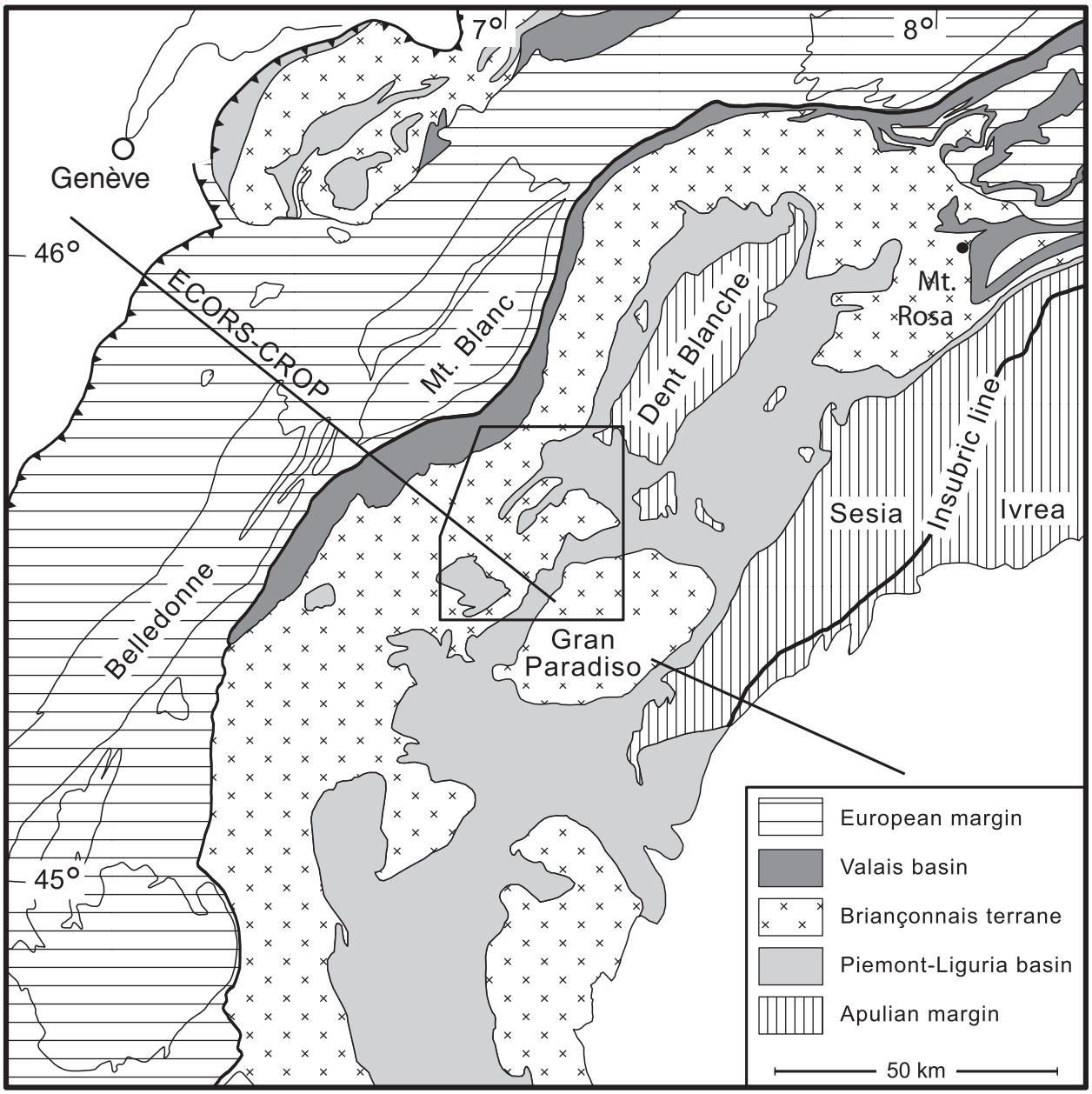

Fig. 1. Paleogeographical domains of the Western Alps after Bucher *et al.* (2003), with the study area outlined. The trace of the ECORS-CROP transect (Roure *et al.*, 1996) is indicated. The black dot indicates the location of additionally analyzed samples from the Monte Rosa nappe.

samples from the study area, including all of the samples dated by ^{39}Ar–^{40}Ar. As white mica is not stable under eclogite-facies conditions in the studied mafic rocks, its formation post-dates the pressure peak. Because it is also clearly seen to pre-date D_2 microstructures, we assign it to a later stage of D_1. In the Internal and Ruitor Units (Fig. 2) the pressures prevailing during D_1 are in the range of 10–14 kbar at *c.* 400–450°C (Fig. 2b; Bucher *et al.*, 2003; Malusà *et al.*, 2005). More externally (internal part of the Zone Houillère Unit close to the tectonic contact with the Ruitor Unit), P–T estimations suggest 5 kbar and 350 ± 25°C, whereas the most external part never exceeded 300 ± 25°C, as indicated by the vitrinite reflectance of coal (Bucher *et al.*, 2003).

North-northwestward nappe stacking and exhumation during D_2 took place under greenschist-facies conditions (Ceriani *et al.*, 2001; Bucher, 2003; Ceriani & Schmid, 2004). D_2 is the dominant deformation event, characterized by isoclinal folds on all scales. Owing to intense transposition the main foliation is usually a composite of D_1

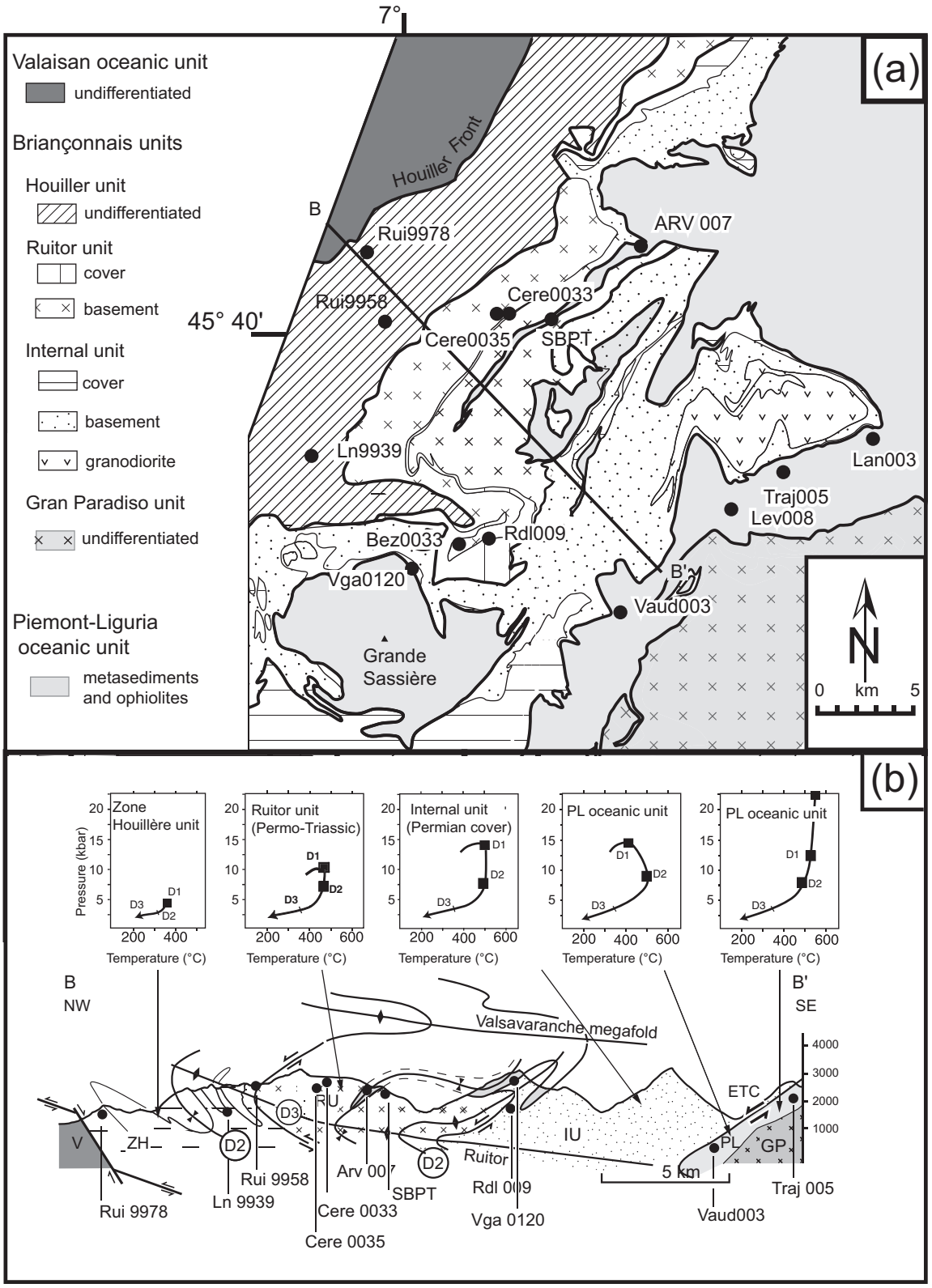

Fig. 2. (a) Geological map of the study area after Bucher *et al.* (2003) showing the locations of the samples. B–B' indicates the trace of the cross-section shown in (b). (b) Schematic cross-section B–B' modified after Bucher *et al.* (2003) and *P–T* path of different tectonic units in the study area. *P–T* conditions were calculated using Geo-Calc software (for details see Bucher *et al.*, 2003; Bucher & Bousquet, 2007). All samples were projected onto this cross-section to show their structural position. V, Valaisan oceanic Unit; ZH, Zone Houillère Unit; RU, Ruitor Unit; IU, Internal Unit; GP, Gran Paradiso massif; P–L, Piemont–Liguria oceanic Unit; ETC, enigmatic tectonic contact.

and D_2. The abundance of the pre-Alpine relicts generally decreases eastwards owing to the eastward increase in D_2 strain magnitude (Bucher *et al.*, 2004). In the external parts of the Ruitor Unit pre-Alpine relicts are common (Baudin, 1987), and they gradually become rare in the internal parts of the Ruitor Unit and in the Internal Unit (Cigolini, 1995).

The last ductile deformation phase, D_3, produced large-scale post-nappe folds (Bucher *et al.*, 2003, 2004); its final stages coincide with a change from top-to-the-NNW to top-to-the-west movements in the Western Alps (Fügenschuh *et al.*, 1999; Ceriani *et al.*, 2001; Ceriani & Schmid, 2004; Loprieno *et al.*, 2011) some 32 Myr ago (Fügenschuh & Schmid, 2003; Simon-Labric *et al.*, 2009). D_3 also developed under greenschist-facies conditions, but in the absence of discrete syn-D_3 mineral parageneses (Bucher *et al.*, 2004) no precise *P–T* estimate for D_3 is possible. The major tectonic contacts are refolded by D_3 (Fig. 2b) and hence must have been formed during D_2. As neither penetrative deformation nor mineral growth occurred during D_3 refolding, it is possible to infer the age of D_2 by dating of syn-D_2 white mica within D_2 mylonites that define these major contacts. Finally, D_3 was followed by continuous cooling to <300–350°C *c.* 30 Myr ago, as indicated by zircon fission-track ages (Malusà *et al.*, 2009).

ANALYTICAL TECHNIQUES

Out of some 150 tectonically and petrologically well-characterized samples, 14 were selected for dating by ^{39}Ar–^{40}Ar incremental heating of white mica. Garnet from three samples was dated by Lu–Hf, and from one sample also by Sm–Nd. To minimize the amount of pre-Alpine relicts, so as to have a good control on processes taking place during the Alpine metamorphic cycle, we avoided the polymetamorphic basement of the Ruitor and Internal Units and selected only monometamorphic rocks for dating. The dataset was designed to be redundant so as to constrain the metamorphic and deformation history of the area, and at the same time to empirically assess the processes that control the K–Ar isotopic system.

Electron microprobe (EMP) analyses were performed at the University of Basel on a JEOL JXA-8600 on thin sections of the samples selected for age determinations. Accelerating voltage was 15 kV, and sample current 10 nA. Representative analyses are shown in Table 2, and the full dataset is reported in Electronic Appendix Table 1 (supplementary data are available for downloading at http://www.petrology.oxfordjournals.org).

All samples were crushed with a jaw crusher and a roll mill, then sieved in different grain size fractions between 125 and 500 μm. The sieve opening is a good approximation of the diameter of the mica platelets. All analysed minerals (white mica, garnet, glaucophane, pyroxene, epidote) were enriched by standard magnetic and gravimetric techniques, then further purified by hand-picking. The detailed procedure of our ^{39}Ar–^{40}Ar analyses has been described by Villa *et al.* (2000). The ^{40}K decay constants followed Steiger & Jäger (1977), and the age of the FCs fluence monitor followed Kuiper *et al.* (2008). A summary of the ages is given in Table 1; the complete dataset is reported in Electronic Appendix Table 2. The Lu–Hf and Sm–Nd procedures followed Kleinhanns *et al.* (2002); the decay constants for ^{147}Sm and ^{176}Lu were taken as 0·00654 Ga^{-1} (Lugmair & Marti, 1978) and 0·01865 Ga^{-1} (Scherer *et al.*,

Table 2: Representative electron microprobe (EMP) analyses of white mica spots imaged in Fig. 5

Traj005	D_1 relict in hinge	D_1 relict in hinge	D_1 relict	D_2 mica	D_2 mica	D_2 mica	D_3 retrogression
SiO_2	52·33	51·74	50·68	49·47	48·71	48·13	45·64
TiO_2	0·22	0·41	0·36	0·58	0·61	0·64	0·05
Al_2O_3	31·74	30·43	28·44	35·20	35·46	34·86	36·23
FeO	2·71	3·21	2·99	1·07	1·42	1·49	0·39
MnO	0·01	0	0·03	0	0·08	0·01	0·03
MgO	1·75	2·1	2·42	0·84	0·8	0·89	0·12
CaO	0	0·02	0·02	0	0·01	0·02	0·12
Na_2O	0·29	0·38	0·30	0·65	1·23	1·15	7·13
K_2O	9·9	9·19	9·08	9·67	8·98	9·11	0·38
musc	0·61	0·55	0·52	0·76	0·78	0·78	0·93
prl	0·16	0·19	0·19	0·13	0·11	0·09	0·03
tri	0·03	0·05	0·04	0	0	0	0
cel	0·22	0·24	0·28	0·14	0·16	0·17	0·04

Calculations of white mica end-member partition follow Bousquet *et al.* (2002); musc, muscovite; prl, pyrophyllite; tri, trioctahedral micas; cel, celadonite. Other EMP analyses are presented in Electronic Appendix Table 1.

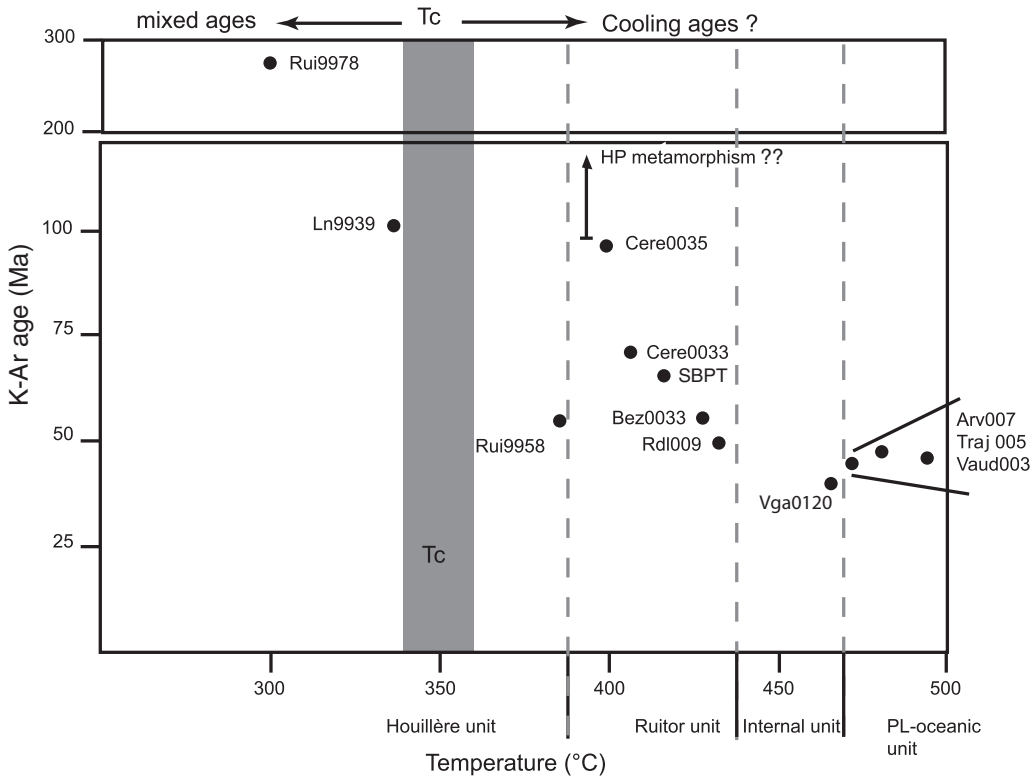

Fig. 3. Dependence of K–Ar (total-gas) ages on metamorphic peak temperature. All units east of the Zone Houillère Unit reached $T > 350°C$. According to 'thermochronology', high-pressure (HP) metamorphism in the Western Alps would be older than the age of the oldest sample east of the grey band, *c.* 100 Ma, and the 40–50 Ma ages of the Internal and P-L Units would imply that the internal parts of the orogen cooled slowly (*c.* 3–5°C Ma^{-1}) between *c.* 100 and 50 Ma. The near-constancy of the K–Ar ages with increasing metamorphic temperature is not explained by 'thermochronology'. Lu–Hf and Sm–Nd ages date prograde garnet growth during the Paleocene–early Eocene and are also incompatible with a Cretaceous HP metamorphism. The paradox can be solved by a detailed study of microstructures and chemical compositions at the micrometre scale, to better understand the factors controlling Ar retention and Ar loss in white mica.

2001), respectively. The complete results are shown in Electronic Appendix Table 3.

AGE RESULTS

The spatial distribution of the ages obtained in this study follows a systematic regional pattern. Figure 3 shows all the K–Ar ages obtained in this study (identical to the ^{39}Ar–^{40}Ar total-gas ages in Electronic Appendix Table 2) plotted against the temperature of Alpine metamorphism, which is independently constrained by petrological data (Bucher *et al.*, 2003). In this section we refer to only ^{39}Ar–^{40}Ar total-gas ages; age spectra and other diagrams displaying Ar isotope systematics will be discussed in a later section. Isochrons can be plotted from the data in Electronic Appendix 2; they will not be further considered, as they do not provide additional information to the stepwise heating age spectra of phyllosilicates (Foland, 1983).

From the most external unit, the Zone Houillère Unit, which underwent the lowest grade Alpine metamorphism, we analysed three samples spanning the entire unit. All three yield total-gas ages ranging between 261 and 51 Ma, from the most external to the most internal sample. The data show a negative correlation between K–Ar (total-gas) age and maximum metamorphic temperature (Fig. 3). A similar correlation was found in the Ruitor Unit, from which five analysed samples give total-gas ages decreasing from 94 to 50 Ma (Fig. 3). One surprising observation is that sample Cere0035 yields a much older total-gas age than Rui9958, despite having been metamorphosed at higher temperature, giving the age–temperature correlation an unpredicted sawtooth pattern. The sample from the Internal Unit has the lowest total-gas age of the whole traverse, 40 Ma. The total-gas ages of the three samples from the P–L Unit are nearly constant (43–47 Ma) and do not correlate with the metamorphic peak temperature.

CONVENTIONAL 'THERMOCHRONOLOGICAL' INTERPRETATION

The conventional 'thermochronological' interpretation (Jäger, 1967) requires that only tectonic units that were heated to $T < 350°C$ may be used for an estimation of the

age of HP metamorphism, because higher-grade white mica should record 'cooling ages' only. In this approach the HP event must always be older than the ^{39}Ar–^{40}Ar mica ages from samples that did not exceed 350°C during Alpine metamorphism. It should be noted that the 350°C 'closure temperature', T_c, of white mica for Ar loss according to Purdy & Jäger (1976) cannot be freely modified, as the entire interpretative edifice that seeks to explain regional patterns of mica ages as 'cooling ages' relies decisively on a tight correspondence to mineral isograds. Any modification of T_c(mica) creates a conflict with this correspondence, causing the whole edifice to collapse (Villa, 1998).

Conventional 'thermochronology' thus requires an age of *c.* 100 Ma for HP metamorphism (i.e. Mid-Cretaceous; 'Eo-Alpine'), with white mica in the Internal and P–L Unit recording post-metamorphic 'cooling'. A difficulty with this interpretation is that the mica 'cooling ages' should decrease eastward as metamorphic grade increases (as it should take longer for higher-grade samples to be exhumed through their 'closure isotherm'), which is not observed (Fig. 3). Most importantly, a supposed Cretaceous eclogitization is incompatible with Lu–Hf and Sm–Nd data on garnet samples from the P–L Unit (Electronic Appendix Table 3), which require a Paleocene–Eocene age for the growth of prograde garnet, and thus an Eocene eclogitic event. Although both the plate motion constraints in the Western Mediterranean and the stratigraphic record in sedimentary basins surrounding the Alps are consistent with an Eocene eclogitic event in the axial belt (Malusà *et al.*, 2011), earlier studies (e.g. Dewey *et al.*, 1989) did not envisage this hypothesis, as the prevailing view for decades had been that eclogites in the whole Alps were of Cretaceous age.

The internal inconsistency of the 'thermochronological' approach at the 100 km scale requires a different approach to interpret the data. We will focus on the mineral geochronometers at the micrometre scale using microchemistry and petrology to constrain the significance of ^{39}Ar–^{40}Ar ages of white mica.

MICROSTRUCTURAL OBSERVATIONS AND EMP ANALYSES OF MULTIPLE WHITE MICA GENERATIONS

To understand the large-scale regional pattern of the white mica ^{39}Ar–^{40}Ar data we need to first understand the role of microstructure and heterogeneous mica composition at the subgrain scale in controlling the Ar isotope record. The different microstructural mica populations were analysed by EMP to relate them to micrometre-scale chemical variations. This procedure allows the chemical fingerprinting of three mica populations: (1) detrital grains; (2) grains formed during D_1; (3) grains formed during D_2. The celadonite content varies significantly in these three populations. The general trend from a dominance of detrital mica in the less deformed external part to the dominance of metamorphic mica in the frequently mylonitic internal part is systematic. The Zone Houillère Unit is dominated by detrital mica in the most external parts of the study area, where metamorphic conditions never exceeded sub-greenschist-facies conditions. Mixed detrital and newly grown mica coexist in the internal part of the Zone Houillère Unit. Even in the immediately adjacent Ruitor Unit inherited grains are still present in all samples, showing that mixed populations are common in the metamorphic portions of orogens, and that detrital mica can survive during subsequent deformation and metamorphism (Bousquet *et al.*, 1998; Agard *et al.*, 2002).

We focus the discussion of the EMP data on the Si content, because it can be used as a geobarometer (Massonne & Schreyer, 1987). In principle, additional indicators can be used to discriminate heterochemical mica generations (e.g. the Mg/Na or F/Fe ratios: Heri *et al.*, 2013), but the Si content is sufficient to illustrate this diversity, with the added bonus of providing qualitative pressure constraints in the higher-grade units. However, in lower-grade units, such as the Zone Houillère Unit, a pyrophyllite component may contribute to high Si contents (Valente & Borghi, 2000).

In the most external part of the Zone Houillère Unit, close to the Houiller Front (Rui9978; Fig. 2a and b), the very weak Alpine foliation is defined by fine-grained mica (Fig. 4a), whereas the detrital mica grains are much larger, show no preferred orientation and are randomly distributed in the matrix (Fig. 4a). The clear textural dichotomy is mirrored by the EMP analyses (Fig. 4b): mica grains identified as detrital on the basis of purely textural criteria have Si contents below 6·4 atoms per formula unit (a.p.f.u.), whereas metamorphic micas have Si contents as high as 6·85 a.p.f.u. At first sight, the Si contents would appear to define a continuous variation between 6·85 and 6·4 a.p.f.u. In fact, the presence of two discrete intergrown mica generations will result in a bimodal Si distribution with two narrow concentration clusters only if the size of the intergrown phases is much larger than the excitation volume of the EMP beam [such as, for example, the sample of Villa (2006, fig. 3)]. If the intergrowth scale is smaller than the excitation volume (Livi & Abad, 2013), a smeared distribution of concentrations and element ratios is obtained (Heri *et al.*, 2013). In that case, the textural context reveals that accurate compositional information is given only by the two extremes of the data distribution.

In the intermediate Zone Houillère Unit the Alpine deformation is more intense. Neocrystallized white mica in sample Ln9939 is still subordinate, but it is larger than in sample Rui9978. Figure 4c shows a three-dimensional

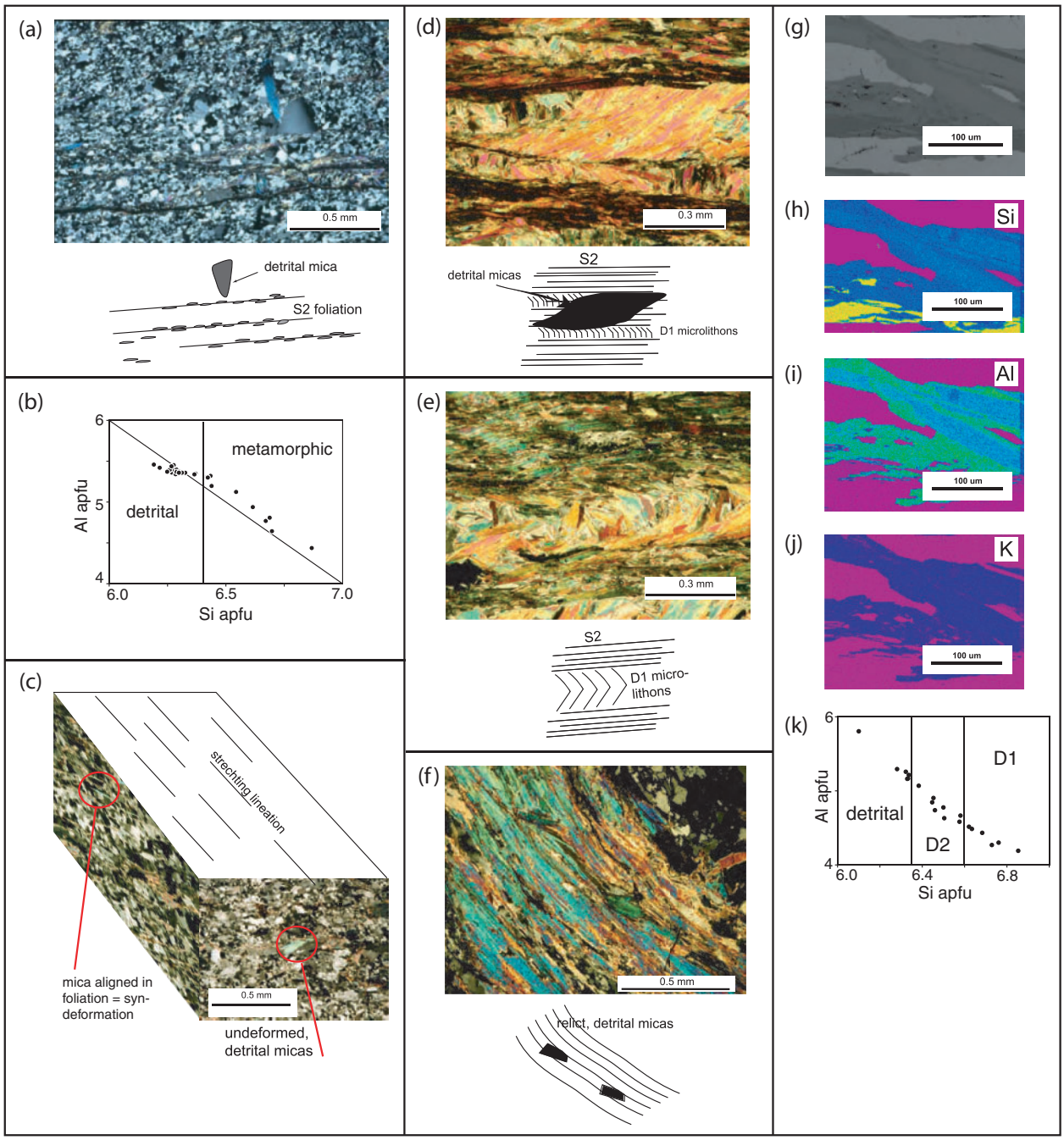

Fig. 4. (a) Thin section of sample Rui9978 from the external Zone Houillère Unit, showing the difference between detrital and metamorphic white mica. (b) Composition of the mica from sample Rui9978 measured by EMP (data in Electronic Appendix Table 1). The limit between the metamorphic high-Si and the detrital low-Si population is based on correlated microstructural and EMP analyses of this study. (c) Three-dimensional distribution of metamorphic and detrital white micas in sample Ln9939 from the intermediate Zone Houillère Unit. (d) Detrital white mica in sample Cere0033. (e) D_1 microlithons in sample Cere0033. (f) Detrital white mica in sample Cere0035. (g) Back-scattered electron (BSE) image of one detrital white mica grain from sample Cere0035 (dark grey). (h) Si false-colour concentration map showing a clear zonation in the detrital mica grains. Blue (highest), green, yellow and red (lowest) represent decreasing concentrations. (i) Al false-colour concentration map verifying the Si zonation. Relative colour coding as in (h). (j) K false-colour concentration map. Relative colour coding as in (h). K concentrations are high across the whole mica grain and show no visible zonation. (k) EMP analyses of the three mica populations in sample Cere0035.

(3D) view of thin sections parallel and perpendicular to the stretching lineation. Newly grown micas are particularly clearly visible in the section parallel to the stretching lineation, where they are well aligned in the foliation. A population of larger and non-aligned grains is best seen in the section perpendicular to the stretching lineation, where they appear together with smaller and well-aligned new micas. Being non-aligned the larger grains are interpreted to be of detrital origin. This sample illustrates that 3D microstructural analysis is needed for accurate interpretation of the age data.

In the Ruitor Unit (Fig. 2a and b) grains belonging to all three identified mica populations are found (Cere0035, Cere0033: Fig. 4d–f). The youngest population, the horizontally aligned micas defining the S_2 foliation (Fig. 4d and e), is interpreted to have recrystallized syn-kinematically with D_2. Microlithons oriented perpendicular to the S_2 foliation (Fig. 4d and e) contain an older population of mica interpreted to have formed during D_1. Much larger grains in comparison with those found within D_1 microlithons and the D_2 micas (Fig. 4d) are interpreted as relict detrital grains and form the oldest population. D_1 micas are also often preserved in fold hinges (Fig. 4e). Sample Cere0035 also contains small detrital grains in addition to the large ones typical in other samples (Fig. 4f). EMP mapping reveals chemical zoning in these smaller detrital micas (Fig. 4g–k).

The P–L Unit exhibits strongly contrasting microstructures as a function of rock competence. We describe here Vaud003, an eclogitic boudin, and Traj005, a calcschist forming the matrix of such eclogitic boudins. Sample Vaud003 was chosen as it predominantly contains D_1 (HP) mica and remained undeformed during D_2: it shows an internal foliation, which is discordant to the main foliation defined by the second phase of deformation (S_2), and hence has to be classified as S_1. The attribution to D_1 is independently confirmed by the mineral assemblage Grt–Px–Qz, implying $P > 15$ kbar. In contrast, calcschist Traj005 is strongly overprinted by S_2 (Fig. 5), and it could appear at first sight that all micas are synkinematic with S_2. However, omnipresent microlithons, relict D_1 fold hinges (Fig. 5a and b) and (large) relict D_1 grains, showing an internal foliation discordant to the main S_2 foliation (Fig. 5c), are clear evidence for the preservation of D_1 relicts. Electron microprobe analyses of Traj005 white micas again show different compositions for different white-mica populations (Fig. 6). A relict D_1-fold hinge (Fig. 6a and b) shows high Si contents (up to 6·8 a.p.f.u.) across the fold hinge, the scatter being part of the apparent variation of the D_1 mica composition whenever the scale of the replacive D_2 mica intergrowth is smaller than the EMP excitation volume (see above). A relict D_1 mica is shown in Fig. 6c–e. The textural difference from the mica of the S_2 foliation is visible in Fig. 5, and is confirmed by the Al concentration map (Fig. 6d). Si contents are >6·45 a.p.f.u. for D_1 mica, whereas they range from 6·15 to 6·40 a.p.f.u. for D_2 mica (Fig. 6b–e). Mica with Si < 6·15 a.p.f.u. postdates the D_2 micas (Fig. 6e), but its occurrence is occasional.

These observations illustrate two general principles, which apply to the entire studied traverse. First, only the inherited micas are zoned, whereas newly formed mica shows no significant compositional heterogeneity. Second, neoformed D_1 and D_2 micas have distinct compositions, suggesting that diffusive re-equilibration of major elements was negligible during Alpine metamorphic events at $450 \pm 25^{\circ}$C. The zoning of detrital mica pre-dates Alpine metamorphism, as confirmed by findings of pre-Alpine parageneses in the Ruitor basement (Baudin, 1987; Giorgis *et al.*, 1999). The chemical differences between the three mica populations (detrital, D_1 and D_2) cause a large spread in mica compositions (Fig. 4k; Electronic Appendix Table 1).

FACTORS CONTROLLING K–Ar AGES

We now compare the insight gained on the petrogenesis of the mica samples with their geochronology. First we present systematic case studies on six selected samples, each illustrating a single issue. We then use the resulting assessment of the respective importance of mixing, diffusion and recrystallization to derive a robust and accurate interpretation of the regional age pattern.

The influence of hand-picking on ^{39}Ar–^{40}Ar ages

To quantify the influence of white-mica purity on ^{39}Ar–^{40}Ar ages we compared the Ar isotope fingerprint of the mechanical separate (magnetic and gravimetric) with its extensively hand-picked counterpart for three samples. Hand-picking is an unquestioned routine practice in many geochronology laboratories, including ours; what we set out to quantify was its effect on samples that are evidently mineralogically heterogeneous. The studied samples represent typical petrogenetic varieties encountered in the area: (1) Ln9939 from the Zone Houillère Unit contains predominant detrital mica grains; (2) Vga0120 from the Internal Unit is a mylonite containing mostly D_2 mica; (3) Traj005 from the P–L Unit contains a mixture of D_1 and D_2 mica populations, lacking detrital grains. Stepwise heating data were obtained on these samples by using very similar laboratory heating schedules. A detailed discussion of these results is presented in Electronic Appendix Text 1; a summary is shown in Fig. 7a–c, which shows that hand-picking indeed generally leads to smaller contamination by extraneous phases degassed in the low-T steps. However, hand-picking may provoke selective

Fig. 5. Thin section of sample Traj005 showing different mica generations (crossed polarizers). (a) Enlargement of a relict D_1 fold hinge. (b) Close-up view of (a); the inset shows the area chosen for the detailed EMP analysis shown in Fig. 6a. Point analyses are given in Table 2 and Electronic Appendix Table 1. (c) Enlargement showing relict detrital mica grains. The location of Fig. 6c is the 200 × 200 μm square outlined between/below (a) and (c).

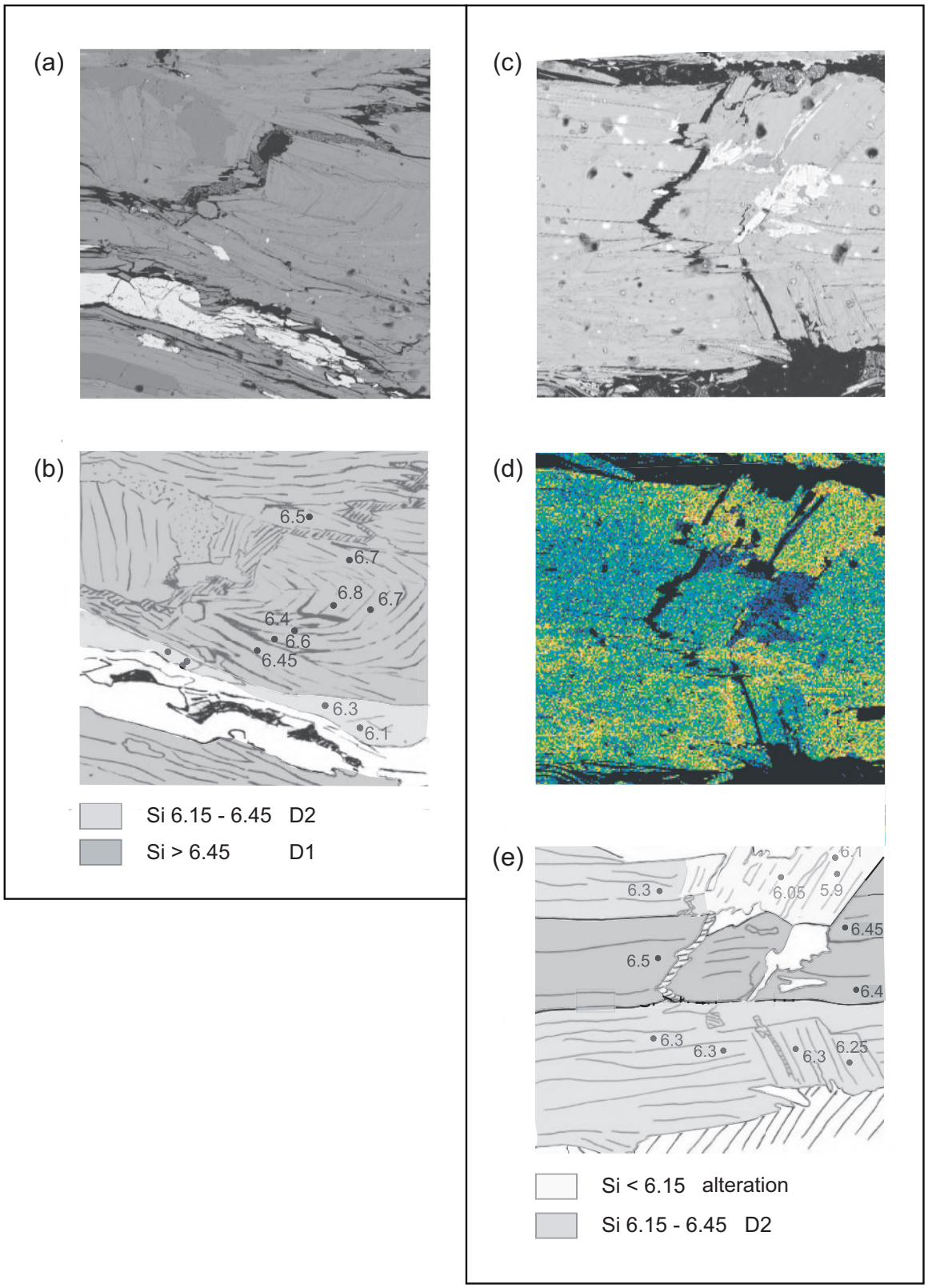

Fig. 6. (a) BSE image of the area shown in Fig. 5b. Field of view 0.3 × 0.3 mm. (b) Contour map of the Si concentration with individual quantitative analyses. (c) BSE image of the area shown in Fig. 5c. Field of view 0.2 × 0.2 mm. (d) Al false-colour concentration map; colour coding as in Fig. 4h. (e) Contour map of the Si concentration. It should be noted that although D_1 mica grains and D_2 mica grains show similar orientation they are texturally different, as is visible in Fig. 5.

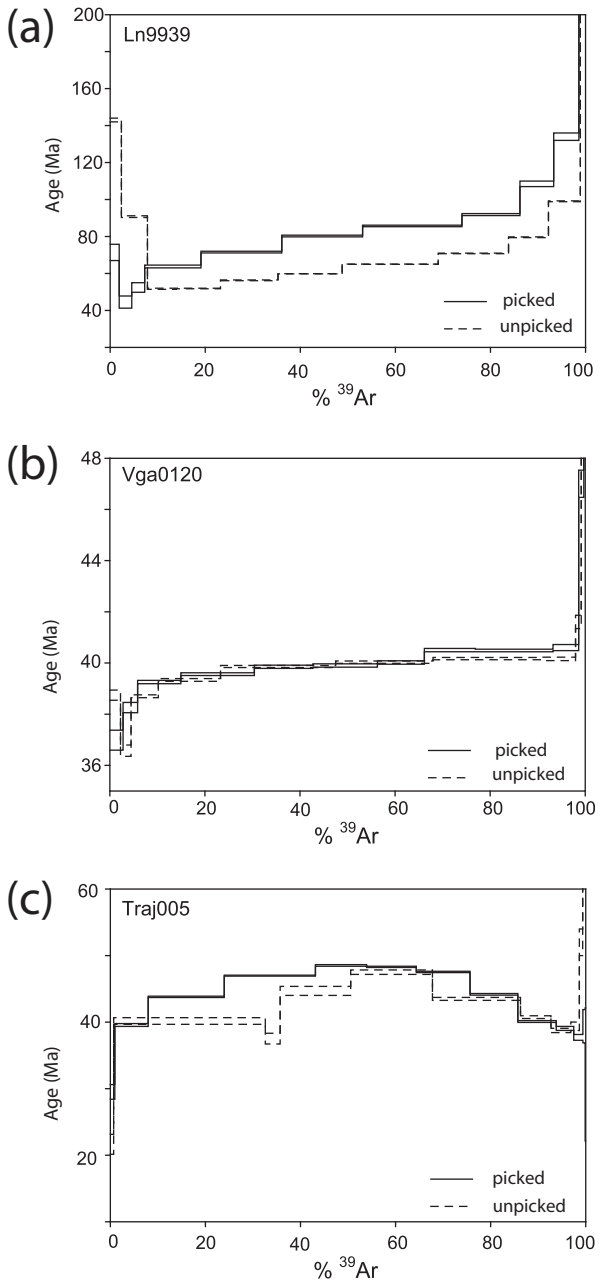

Fig. 7. Age spectra comparing picked and unpicked mica fractions; the grain size for all fractions was 125–160 μm. (a) Ln9939. The hand-picked aliquot consistently yields step ages that are older by 10–15 Ma than the unpicked aliquot, suggesting a subjective sampling bias. (b) Vga0120. This single-generation D_2 mica shows no major differences in the age spectra between picked and unpicked aliquots, except for the first two steps. As for Ln9939, this difference is best explained by the contamination of Cl-rich minerals other than mica in the unpicked aliquot. (c) Traj005. The age spectra of both aliquots display an upward-convex shape. As established by Wijbrans & McDougall (1986), this pattern clearly identifies two mica populations, whereby the oldest step of the age spectrum of a mixture defines the minimum age for the older phengite population and the youngest steps define the maximum age for the muscovite population. The width of the 'hump' pertains to the mass balance between the D_1 and D_2 generations. It appears that hand-picking of Traj005 has enriched D_1 phengite preferentially.

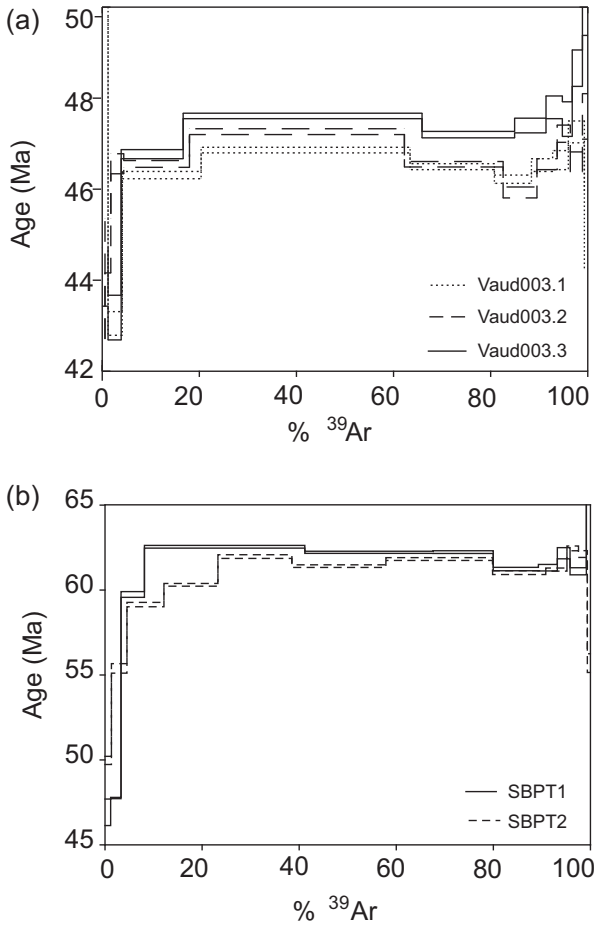

Fig. 8. (a) Age spectra of samples Vaud003.1, Vaud003.2 and Vaud003.3; the sieved size fractions are 125–160 μm, 160–250 μm and 250–500μm, respectively. The age spectra are almost parallel, with an age difference of *c.* 0·5 Ma. (b) Age spectra of samples SBPT1 and SBPT2; the size fractions are 160–500 μm and 125–160 μm respectively. The two age spectra coincide within 1 Ma over 80% of the ^{39}Ar release.

enrichment if two populations are present. In particular, if the age difference between the two populations (detrital pre-Alpine and Alpine mica) is large, hand-picking may lead to unrepresentative results (see Villa, 2006, p. 166).

The influence of grain size on ^{39}Ar–^{40}Ar ages

To test the role of diffusion, we dated different grain-size fractions of white mica taken from two samples that reflect entirely different processes (Fig. 8). Sample Vaud003 almost exclusively consists of D_1 phengite grown during eclogite-facies metamorphism and its age is expected to mirror the closure to Ar loss (independently of the exact Ar-loss mechanism, which will be discussed below) at, or after, the metamorphic peak. Sample SBPT, on the other hand, is dominated by detrital mica; its age is controlled

by (partial) resetting of the ages of pre-Alpine grains. If diffusive Ar loss had played an important role during either exhumation or rejuvenation, different ages for different grain sizes would be expected, whereby it is necessary to ensure that (1) the sieve fraction reflects natural grain size and not just mechanical comminution of a uniform size distribution larger than the largest analysed grain size, and (2) the effective grain size controlling diffusion is larger than the smallest analysed grain size. Point (1) holds true for our samples, whose natural grain-size variations range from >500 to <50 μm. Point (2) also holds true, as it is well known (Villa *et al.*, 1996, and references therein) that the effective grain size for diffusion coincides with the crystallographically coherent mineral structure, which in the present case coincides with the whole grain.

Sample Vaud003 is an undeformed eclogitic boudin, as described above. The analysed grain-size fractions were 125–160 μm (Vaud003.1), 160–250 μm (Vaud003.2) and 250–500 μm (Vaud003.3). The corresponding age spectra are nearly identical (Fig. 8a), all spectra displaying a weak but statistically significant upward-convex shape; this fingerprint of heterochemical mica generations can be used to qualitatively estimate the relative abundance of phengite and muscovite. In this sample phengite is predominant and muscovite is subordinate; each size fraction is (slightly) heterochemical. The almost identical age spectra for all three size fractions rules out that ^{40}Ar inherited from detrital grains and 'excess' ^{40}Ar play an important role; diffusion theory would predict the grains with different radii to be affected to different degrees. We also point out that whenever recrystallization is only partial, the smallest grains are most affected by it; the effects of diffusion and of recrystallization parallel each other.

In each size fraction of sample Vaud003, the steps most closely representing D_1 phengite are identified on the basis of two criteria: their position as the oldest steps of the hump-shaped age spectra (Wijbrans & McDougall, 1986), and their nearly constant Cl/K ratio of $4–5 \times 10^{-4}$. In all three size fractions these criteria are met by the 760°C step, which accounts for over 40% of the ^{39}Ar release in each fraction. The 760°C steps of the three size fractions display a small but significant, regular age difference: for the smallest, intermediate, and largest grain size (Vaud003.1, Vaud003.2 and Vaud003.3) the respective ages are $46{\cdot}86 \pm 0{\cdot}06$ Ma, $47{\cdot}27 \pm 0{\cdot}07$ Ma, and $47{\cdot}61 \pm 0{\cdot}06$ Ma (Electronic Appendix Table 2).

The age comparison between size fractions of Vaud003, whose median grain radii vary between 71 and 187 μm, allows the calculation of the role of diffusion. The maximum possible diffusivity can be constrained in the limiting case of zero recrystallization (even if in fact this deformed sample contains multiple, heterochemical, recrystallized mica generations). A mathematical formulation of Ar retention is provided by the equations of Dodson (1973) defining T_c for Ar loss as a function of the activation energy, E, the diffusion coefficient at infinite T, D_0, and the cooling rate, dT/dt. The quantification of the diffusion parameters, however, is problematic. As hydrothermal laboratory experiments with added water always are subject to recrystallization of the experimental charge (Hess *et al*, 1987; Villa & Puxeddu, 1994; Harrison *et al*, 2009), their results are not applicable to those natural systems for which an estimate of the true volume diffusivity is required. To derive the latter, it is necessary to infer it from indirect evidence.

The diffusivity of Ar in white mica has been constrained by the case study by Hames & Cheney (1997) of a polymetamorphic, centimetre-sized muscovite porphyroclast. Those authors showed that Ar diffusion is very slow. From the data of those researchers, Villa (2010, p. 10) calculated that the diffusion coefficient D ranged between 4×10^{-21} and 4×10^{-20} cm^2 s^{-1} at *c.* 450°C. This agrees with the estimation of Graham (1981), based on an experimental study on the diffusion coefficient of hydrogen, who argued that D(Ar) must be orders of magnitude smaller than the estimated D(H) at 450°C, 10^{-19} cm^2 s^{-1}. This Ar diffusion coefficient can be used to calculate a T_c following Dodson (1973).

The equation of Dodson (1973) contains four unknowns: T_c, E, D_0 (or, as we shall discuss below, its P-adjusted equivalent, D'_0) and dT/dt. If T_c and E can be independently constrained on the basis of field estimates, the other two follow from the given boundary conditions. In the case of Vaud003, the boundary condition is provided by the grain-size fractions: the sample having $a = 0{\cdot}0187$ cm is older than that having $a = 0{\cdot}0071$ cm by $0{\cdot}75 \pm 0{\cdot}08$ Ma. The cooling rate that results from the difference in the calculated T_c for Vaud003.3 and Vaud003.1 divided by their age difference is iteratively fed into the equation of Dodson (1973).

As starting values we choose $T_c = 500$°C and $E = 250$ kJ mol^{-1}. The former value was established in a field study in the Central Alps (Allaz *et al.*, 2011) for samples that record a pressure of *c.* 7–8 kbar. It may be a conservative underestimate, as retention of ^{40}Ar in white mica near or above 550°C is well documented in the literature (Hammerschmidt & Frank, 1991; De Sigoyer et al., 2000; Di Vincenzo *et al.*, 2001, 2004; Philippot *et al.*, 2001; Villa, 2006; Warren *et al.*, 2012). If we take into account a pressure dependence of T_c of 6–7°C kbar^{-1} (Dahl, 1996*a*), in the present samples T_c would increase by *c.* 40–50°C relative to the Barrovian muscovites from the Central Alps. The value for E is based on the phlogopite diffusivity data of Giletti (1974), increased slightly to take into account the lower ionic porosity of muscovite compared with phlogopite (Dahl, 1996*b*). Our aim is to derive the diffusivity for geologically realistic situations; therefore, we can introduce the pressure-adjusted diffusion coefficient, D',

which already incorporates the pressure dependence for the natural conditions studied by Allaz *et al.* (2011). This has the advantage of a greater robustness with respect to possible systematic errors in the estimate by Dahl (1996*a*) of the pressure dependence. Very few muscovites will record pressures <8 kbar at 500°C; this means that very few natural muscovite samples have a diffusivity higher than that calculated here. For muscovite formed in the 8–16 kbar range, the systematic bias will only be at most half of any possible bias of the estimate of Dahl (1996*a*).

The calculated values of D'_0 and T_c are 0·1 $cm^2 s^{-1}$ and 494°C, respectively, for sample Vaud003.3. The calculated T_c for Vaud003.1 is 460°C, lower by 34°C than that of the coarser size fraction. The resulting 'cooling rate' during the initial post-eclogitic decompression stage is thus 45 ± 5°C Ma^{-1}. The combination of the values for D'_0 and E assumed here can be extrapolated to temperatures of geological interest (e.g. 450°C). Our D'_0 and E predict a diffusivity $D'_{450°C} = 10^{-19·1}$ $cm^2 s^{-1}$. This value is too high, as it is identical to the diffusivity of hydrogen in muscovite (Graham, 1981), and higher by a factor between two and 20 than the diffusivity of Ar calculated from the muscovite of Hames & Cheney (1997) (Villa, 2010, p. 10). This suggests that the starting values for T_c and E we used for our simple model calculation actually overestimate the diffusivity of Ar. Reducing D'_0 by half an order of magnitude, $D'_0 = 0·03$, leads to $T_c = 519$°C and 482°C in Vaud003.3 and Vaud003.1, respectively. The additional P-dependent increase of T_c by ≥ 40°C (see above) means that the T_c for the coarsest and finest size fractions is 560°C and 520°C, respectively, higher than or equal to the temperature prevailing during the metamorphic peak (500 ± 30)°C. This suggests that the apparent age difference between the small and the large grains reflects, at least in part, the preferential preservation of non-retrogressed cores in the larger grains. Taking into account that the partial retrograde recrystallization in Vaud003 (which we had set to zero when modelling all Ar losses as if they had been diffusive) has the effect of decreasing the importance of diffusion, further reducing D'_0, which will lead to even higher T_c. We thus conclude that the age of the metamorphic peak is very closely approximated by fraction Vaud003.3 at 47·61 ± 0·06 Ma, with a total systematic uncertainty smaller than 1 Ma.

Finally, the hypothesis that Vaud003 might provide a record of ^{40}Ar diffusion needs to be reconciled with the observation that the shape of the spectra of the three grain-size fractions does not change as a function of incomplete ^{40}Ar retention. Not even the smallest grain size shows a staircase-shaped age spectrum, which is often viewed as a reflection of diffusive Ar loss. In fact, it is well known that *in vacuo* degassing of phyllosilicates does not mirror the geometrical distribution of ^{40}Ar in the crystals (Hodges *et al.*, 1994), and that staircase-shaped spectra instead originate from a mixture of two diachronous mineral generations (Villa & Hanchar, 2013).

Sample SBPT, the second sample analysed for grain-size effects, was collected from the Permo-Triassic cover of the Avise synform, near the contact between the Ruitor Unit and the P–L Unit (Fig. 2; Caby, 1996). The analysed grain-size fractions were 160–500 μm (referred to as SBPT1) and 125–160 μm (SBPT2). The two total-gas ages are indistinguishable (61·0 ± 0·1 and 60·9 ± 0·1 Ma). The age spectra are similar, yielding two geologically meaningless plateaux at 62–63 Ma (Fig. 8b; see also Electronic Appendix Text 1). During the Eocene HP event, resetting the detrital mica population purely by volume diffusion would require much longer than 500 Myr, implying that diffusion of ^{40}Ar has been negligible in controlling the Ar isotope record of sample SBPT. Similar conclusions had already been reached by Foland (1979), Chopin & Maluski (1980), Chopin & Monié (1984) and Monié (1985).

In cases where Ar diffusion is slow, ^{40}Ar inheritance is expected. In turn, if inherited ^{40}Ar plays a significant role, the K–Ar age is not that of the metamorphic crystallization, but is excessively old. Accordingly, Lanphere & Dalrymple (1976) gave a rigorous definition of the terms 'inherited ^{40}Ar' and 'excess ^{40}Ar'. Inherited ^{40}Ar was produced by ^{40}K decay in the mineral's prehistory and was never completely lost during the formation of the mineral observed at present. Excess ^{40}Ar was introduced into a mineral during or after its formation. These two terms describe two entirely different geochemical processes: the former amounts to (partial) ^{40}Ar loss, the latter to ^{40}Ar gain. Nevertheless, Kelley (2002) proposed to explain all data that deviate from the assumption by Jäger (1967) of very high diffusivities and very low T_c by excess ^{40}Ar, thereby clouding the profound difference between ^{40}Ar loss and introduction of ^{40}Ar from outside. 'Excess ^{40}Ar' often becomes a term used to explain problematic ages (in the absence of multichronometric controls). Unfortunately, the choice of what ages are defined as 'problematic' merely depends on the chosen value for T_c; by doing so one effectively follows a circular argument. We propose that, because mixed ages are normal for minerals that grew below their T_c, a shift of T_c to higher T changes 'problematic' ages attributed to excess ^{40}Ar to normal mixed ages with inherited ^{40}Ar, but without excess ^{40}Ar. The distinction between excess and inherited radiogenic isotope concentrations is not merely a semantic one, but one of essence. It can be achieved by multichronometric control [e.g. comparing the K–Ar and Rb–Sr systems (Villa *et al.*, 2006), or the K–Ar and Lu–Hf systems, as done here], which immediately eliminates the ambiguities inherent in the use of a single isotopic system. It can also be achieved by correlating the chemical and microstructural evidence for petrological relicts with the isotope record.

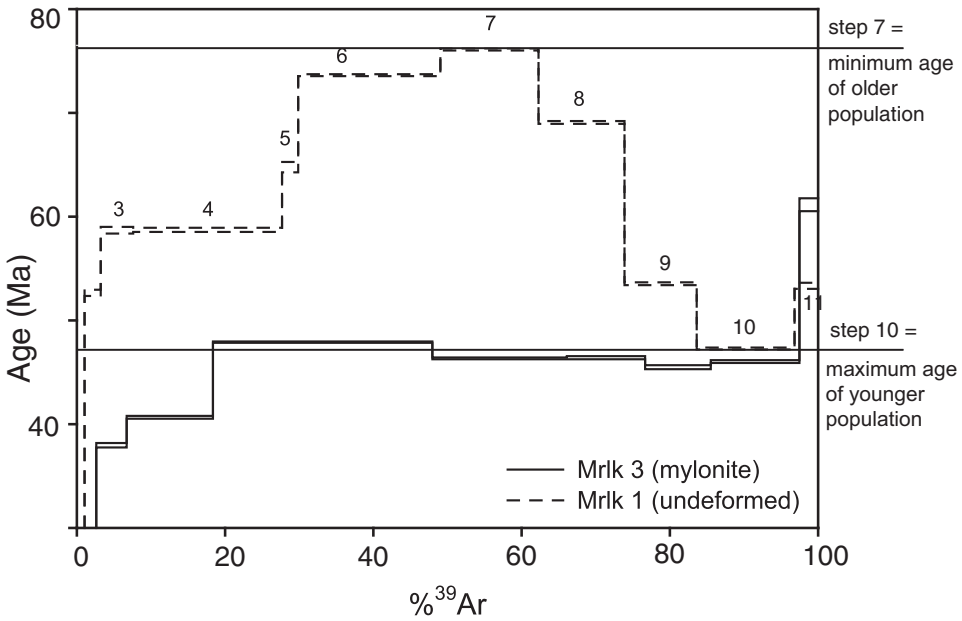

Fig. 9. ^{39}Ar–^{40}Ar age spectra of two samples from the Bottarello glacier, Monte Rosa nappe. Both samples belong to the same host-rock and were collected 1 m apart. Mrlk1 shows an upward-convex age spectrum, typical of a mixture of two diachronous white micas. Mrlk3 shows a much flatter age spectrum between 48 and 46 Ma. The coincidence of the plateau age of Mrlk3 with the maximum age for the younger population of Mrlk1 suggests that the same *c.* 48 Ma mica population that predominates in Mrlk3 is also present in Mrlk1, but not exclusively. The behaviour of the ^{39}Ar–^{40}Ar isotopic system cannot be explained by thermal criteria and can be correctly predicted only by the microstructural observation that mylonite sample Mrlk3 amost exclusively consists of Alpine mica, whereas Mrlk1 was little deformed during the Alpine orogeny. Keller *et al.* (2004) observed pre-Alpine relicts only in Mrlk1.

The influence of deformation on ^{39}Ar–^{40}Ar ages

Two samples from the Bottarello glacial cirque (Monte Rosa nappe) were analysed to examine the influence of deformation on ^{39}Ar–^{40}Ar ages. The median temperature in the investigated part of the Monte Rosa nappe during the early stages of Alpine metamorphism was ~650°C (Engi *et al.*, 2001). According to the T_c approach, the ^{39}Ar–^{40}Ar ages should date the time when these samples cooled below 350°C during exhumation. As samples Mrlk1 and Mrlk3 were collected about 1 m apart (Table 1), they should be the same age. Instead, Mrlk1 has a hump-shaped age spectrum (Fig. 9) and a total-gas age of 62·9 ± 0·3 Ma, whereas Mrlk3 has a much flatter age spectrum and a total-gas age of 45·9 ± 0·3 Ma. This age difference was not caused by the thermal history and can be explained only by the petrological differences. Mrlk1 was taken from the pre-Alpine wall-rock of a shear zone and largely preserves the pre-Alpine paragenesis, whereas Mrlk3 was taken from the shear zone itself (Keller *et al.*, 2004, fig. 2); its garnet–phengite–paragonite assemblage was formed during HP shearing or recrystallization. We therefore consider *c.* 48 Ma as a reliable age estimate of D_1 deformation in the relevant sector of the Monte Rosa nappe (see Electronic Appendix Text 1).

The comparison of these two samples indicates that at a metamorphic peak temperature ≥600°C (Engi *et al.*, 2001; Keller *et al.*, 2004) Mrlk1 retained some of its ^{40}Ar whereas Mrlk3 retained none. This proves that petrological, structural and microstructural control is essential in determining whether or not mica will retain inherited ^{40}Ar during recrystallization. Attributing the inheritance of pre-metamorphic ages at $T > 400$°C only to the lack of an intergranular Ar sink (Warren *et al.*, 2012) does not explain the context of the present samples. First, the diffusivity of Ar in white mica assumed by Warren *et al.* (2012) is unrealistically high, as the hydrothermal laboratory experiments with added water cannot separate the effects of diffusion from Wood–Walther dissolution–reprecipitation (Villa, 2010, pp. 5–6) and, therefore, must not be exported to the geological reality. Second, the observation that sheared sample Mrlk3 gives an Eocene age, unlike Mrlk1, may well be compatible to some extent with different intergranular fluid conditions. However, what is most obvious in the comparison between Mrlk1 and Mrlk3 is that the mineral composition of the sheared sample is different from that of the unsheared one, which is certain evidence of recrystallization.

For T to be the only parameter controlling isotope exchange, the T_c of a mineral would need to be lower than the lower boundary of the stability field of that mineral. This leads to a natural classification of mineral geochronometers into two classes.

'Class I' chronometers are those minerals for which T_c is lower than the stability field of the mineral; diffusion is

fast enough to reset the isotopic clock constantly during mineral growth, so that old inherited minerals and newly grown ones have the same age signatures at any time. They never display heterochronous generations, as all grains grew above T_c. Examples are fission-track and (U + Th + Sm)–He chronometers.

'Class II' chronometers are those minerals for which T_c is higher than the lower boundary of the mineral's stability field. In Class II minerals, heterochronous generations coexist as overgrowths without isotope resetting, and polygenetic disequilibrium assemblages retain their isotopic disequilibrium. Within-grain disequilibria (*sensu* Villa & Williams, 2013) have been documented for biotite, K-feldspar, monazite, muscovite and zircon (and most other mineral geochronometers as well). This means that these minerals are all Class II chronometers.

Temperature does play a role in enhancing reaction kinetics, leading to more or less thorough recrystallization of a mineral (including dissolution–reprecipitation, new growth, reaction). However, T is not the sole parameter uniquely controlling isotope transport. The age of a Class II mineral, as defined above, cannot be used to solve the inverse problem ('given a fractional loss, what was the temperature that caused this loss?'), as thermally activated diffusion is always slower than competing processes such as fluid-induced recrystallization and deformation-induced recrystallization (Cole *et al.*, 1983; Lasaga, 1986; Villa, 1998, 2006, 2010; Allaz *et al.*, 2011; Villa & Williams, 2013).

REGIONAL PATTERN OF MICA AGES

Zone Houillère Unit

Samples from the Zone Houillère Unit consist of a mixture between metamorphic and detrital mica populations. Partial recrystallization and ensuing preservation of detrital mica is also revealed by staircase-shaped spectra (Fig. 10a, c and e), by the tell-tale anticorrelation of Cl/K with age (Fig. 10b and f), and by the EMP analyses (Fig. 10d; see also Electronic Appendix Text 1).

Ruitor Unit

The increase in intensity of deformation towards the SE continues across the Ruitor Unit and is responsible for a decreasing amount of detrital pre-Alpine mica and an increasing amount of metamorphic mica. All samples from the Ruitor Unit contain multiple mica generations. The age spectra of the five analysed samples (Fig. 2) show common features (Fig. 11a).

Samples Cere0035 and Rdl009 display staircase-shaped age spectra. The mixture between Alpine metamorphic mica and pre-Alpine detrital grains indicated by our petrological and microstructural observations (see also Baudin, 1987; Giorgis *et al.*, 1999) is confirmed by the variations in Cl/K (Fig. 11b). In contrast, Cere0033, SBPT and BEZ0033 display 'plateau' age spectra. As discussed above, these apparent 'plateaux' are artefacts due to the simultaneous degassing of two generations of mica, an inherited one and an Alpine metamorphic one, which in this series of samples degas over very similar temperature intervals. A precise quantification of the 'end members' on the basis of the age spectrum alone is impossible, as already demonstrated by Hodges *et al.* (1994). Total-gas ages of single samples show a systematic eastward decrease from 93 Ma to 55 Ma in relation to their structural position (Fig. 11a). To display the common patterns of these mixtures, all samples are plotted together in a Cl/K vs age correlation diagram (Fig. 11b). The data define a minimum triangle with vertices defined by the envelope of all steps of all samples. The resulting ages of the three vertices, interpreted to represent the three microstructurally observed populations, can be visually estimated from Fig. 11b. The vertex corresponding to the oldest age suggests an apparent age of *c.* 135 Ma for the inherited (detrital) mica. This is younger than the age of the inherited population of sample Rui9978, suggesting that the pre-Alpine micas in the Ruitor zone were partly recrystallized. This is supported by the microstructural observation of chemically zoned detrital mica grains. The vertex with the highest Cl/K ratio defines an age of *c.* 47–50 Ma, which is compatible with the observation from sample Rdl009, and it is interpreted to represent the age of D_1. The vertex corresponding to the lowest age points to a population with an age of *c.* 40 Ma, compatible with the estimate for D_2 provided by sample Vga0120 discussed below.

Internal Unit

Vga0120 is a mylonitic Triassic quartzite collected at the tectonic contact between the Internal Unit and the P–L Unit (Fig. 2). These mylonites formed during D_2 (Bucher *et al.*, 2003, 2004). Our microstructural and chemical data show neither an abundant inherited mica population nor substantial retrogression. Therefore, the age of this sample can be interpreted as the age of D_2. The age spectrum is almost flat, with slightly increasing ages (Fig. 7b). In the literature the average of such a quasi-flat age spectrum is sometimes interpreted as a reliable plateau age (e.g. Dal Piaz *et al.*, 2001), despite small but significant differences of the step ages. The Cl/K–age correlation diagram (Fig. 12) reveals a V-shaped trend, indicating heterochemical mixtures of three components. This requires that only the step with the end-member chemical signature should be considered as closely approximating the true age of one specific reservoir and not the average of several heterochemical steps.

The crystallization age of the D_2 mica in sample Vga0120 is estimated from the steps with the lowest Cl/K ratio (940°C in both hand-picked and unpicked

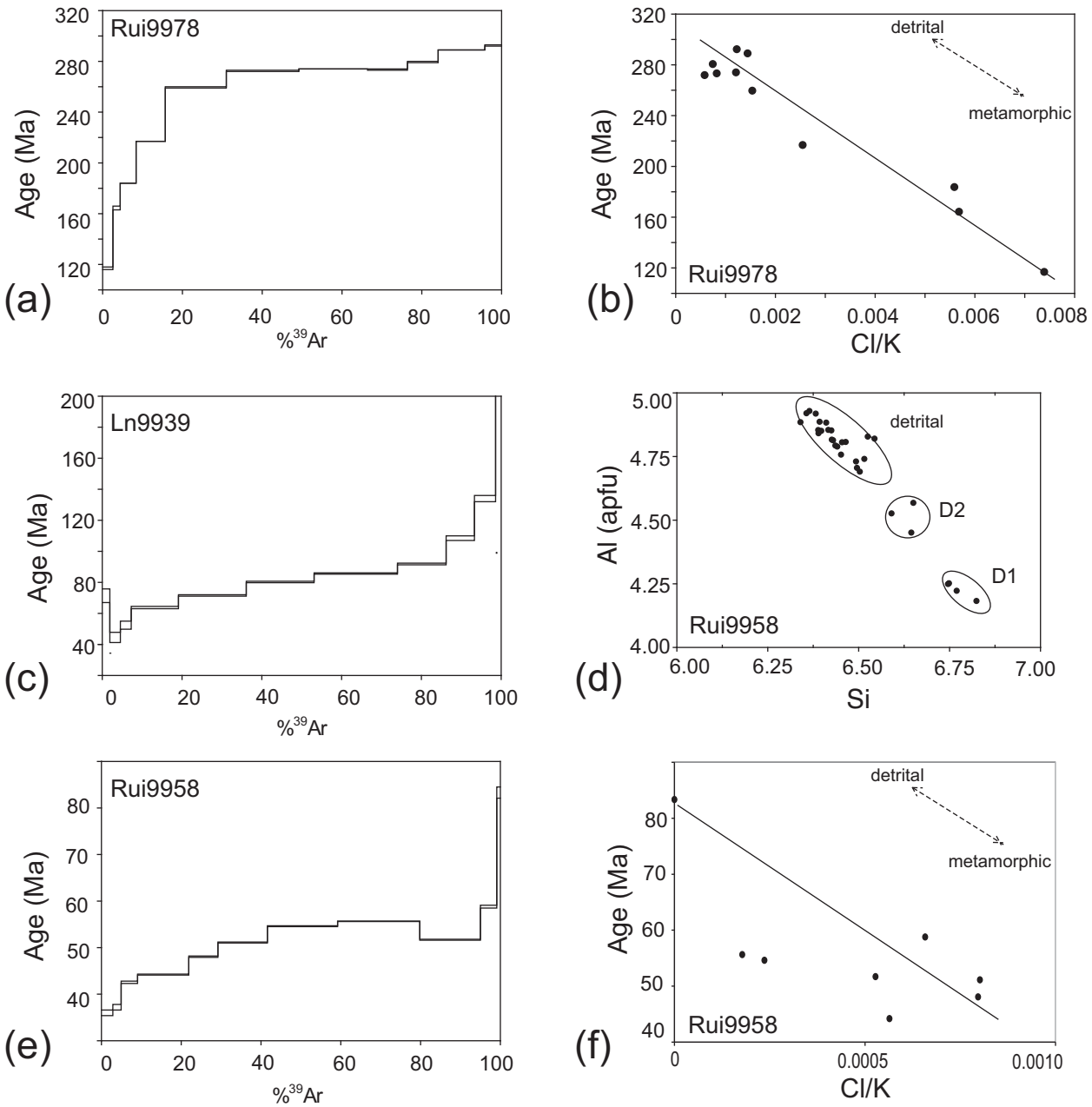

Fig. 10. ^{39}Ar–^{40}Ar results from the Zone Houillère Unit. (a) Staircase-shaped age spectrum of sample Rui9978, with a youngest step at 116·9 ± 0·8 Ma and step ages continuously increasing up to 292·2 ± 0·5 Ma. In the literature such staircase-shaped age spectra are sometimes described as being due to diffusive loss (e.g. Markley *et al.*, 1998). However, it is known that intra-grain age gradients in mica result in plateaux, not staircases (Hodges *et al.*, 1994). Instead, staircases such as that of (a) are best interpreted as mixed ages. A pre-Alpine detrital mica population with an age ≥292 Ma is mixed with an Alpine metamorphic population. (b) Cl/K–age correlation diagram for Rui9978. The negative linear correlation is evidence for a binary mixture between heterochemical, diachronous mica populations (Villa, 2001). (c) Staircase-shaped age spectrum of sample Ln9939. (d) Mica compositions of sample Rui9958: EMP analyses reveal different mica populations. (e) Staircase-shaped age spectrum of sample Rui9958. (f) Cl/K–age correlation diagram. As in (b), the negative correlation is evidence for a binary mixture.

aliquots) as 39·7 ± 0·1 Ma. The three steps defining an apparent 'plateau' in Fig. 7b (steps 5–7 of the hand-picked fraction; Electronic Appendix Table 2) have Cl/K ratios of $(1{\cdot}5–2{\cdot}3) \times 10^{-4}$, much higher than that $(1{\cdot}9 \times 10^{-5})$ of the 940°C step, which we used to infer the D_2 vertex. This means that these three steps contain a detectable proportion of Ar from the D_1 mica and/or D_3 retrogression phases, making the 'plateau' statistically valid but petrologically meaningless. We conclude that the clear attribution of this quartzite mylonite to D_2

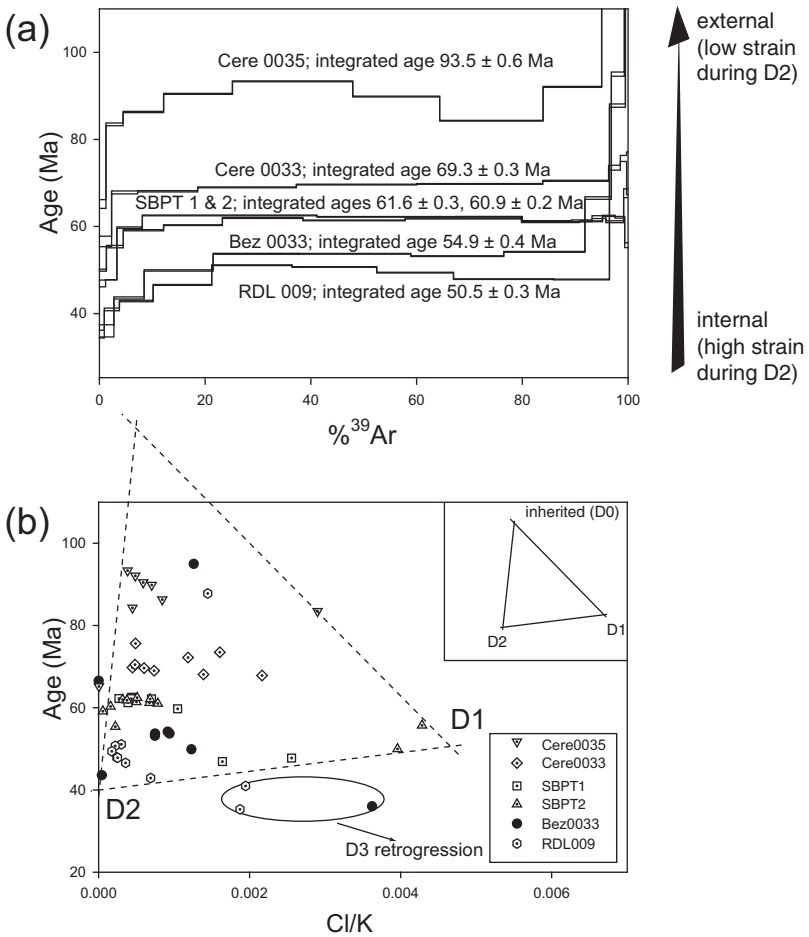

Fig. 11. ^{39}Ar–^{40}Ar results from the Ruitor Unit. (a) Age spectra of all samples from the Ruitor Unit. The relationship between structural position and integrated age should be noted. The apparent 'plateaux' of samples SBPT1 and Bez0033 are geologically meaningless, as they represent mixtures between Alpine metamorphic mica and an inherited component. (b) Cl/K–age correlation diagram. The three vertices point to an age of 47 ± 1 Ma for D_1, 40 ± 1 Ma for D_2 and an inherited component with a geologically meaningless apparent age of about 135 Ma. The three youngest step ages are interpreted as Cl-rich D3 retrogression.

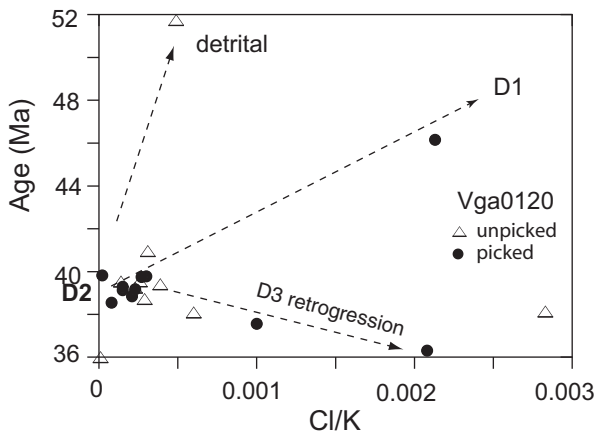

Fig. 12. ^{39}Ar–^{40}Ar results from the Internal Unit: Cl/K–age correlation diagram for syn-D_2 mylonite sample Vga0120 (see age spectrum in Fig. 7b), pointing to a vertex at *c.* 40 Ma for syn-D_2 mylonitization.

suggests an age of 39·7 ± 0·1 Ma for D_2 in the Internal Unit.

Piemont–Liguria Oceanic Unit (Schistes lustrés)

The age of late D_1, closely approximating the metamorphic peak, can be estimated as *c.* 47·6 Ma on the basis of eclogitic boudin Vaud003 (Fig. 8a), which contains an almost pure D_1 mica population. In contrast, calcschist Arv007 contains both D_1 and D_2 mica populations (Fig. 13a and b), whose ages can be estimated from the Cl/K correlation diagram as *c.* 39·5 Ma for the younger and ≥45·4 Ma for the older population.

The Cl/K–age correlation diagram for Traj005 (Fig. 13c) indicates ages of *c.* 48 Ma for D_1 phengite and of *c.* 40 Ma for D_2 muscovite. The end-member determination in the Cl/K–age diagram and the visual estimation of the age

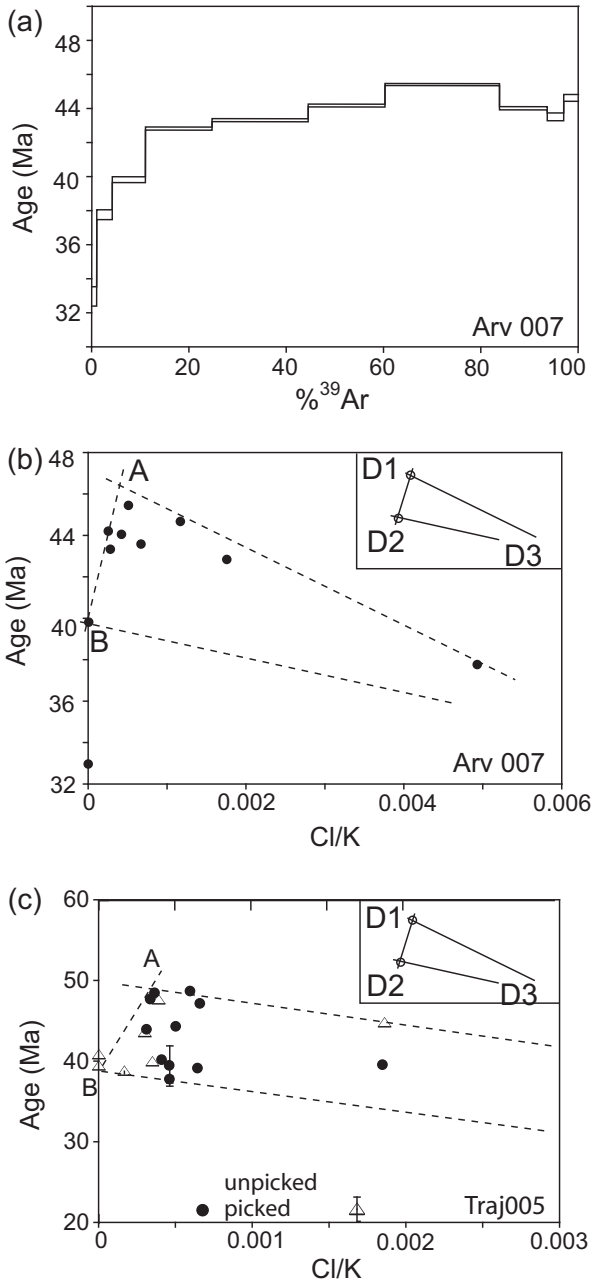

Fig. 13. ^{39}Ar–^{40}Ar results from the P–L Unit. (a, b) Age spectrum and Cl/K–age diagram of sample Arv007. Vertex A represents the D_1 phengite population and vertex B the D_2 muscovite population, with ages of *c.* 47 and *c.* 40 Ma, respectively. (c) Cl/K–age correlation diagram for sample Traj005, indicating a D_1 population of *c.* 48 Ma (vertex A) and a D_2 population of *c.* 40 Ma (vertex B). In (b) and (c), D_1 HP phengites have higher Cl/K ratios than D_2 greenschist retrogressive muscovite grains.

spectrum (Fig. 7c) following Wijbrans & McDougall (1986) give identical estimates for the D_2 age.

When studying the mixed D_1–D_2 micas by using Cl/K–age correlations it is observed that the end-members with ages of 47–48 Ma have higher Cl/K ratios than those with ages around 40 Ma (Fig. 13b and c). It is especially remarkable that eclogitic fluids have often been documented to be hypersaline (Frezzotti *et al.*, 2004, p. 212), which gives further support for our identification of high-Cl/K mica as the HP D_1 generation. Additional effects, such as a high partition coefficient for Cl in HP mica (Nazzareni *et al.*, 2008; J. Glodny, personal communication, 2013), can increase the effect of fluid chemistry.

In the samples from the Internal and P–L Units we found no detrital mica. Samples containing two populations of heterochemical Alpine metamorphic mica can be unravelled to give end-member ages for D_1 (*c.* 47–48 Ma) and D_2 (*c.* 40 Ma). These end-member ages coincide with the ages of samples having a single predominant population (Vaud003, Vga0120), which accordingly are characterized by flat age spectra (Fig. 14). We find no indications for excess or inherited ^{40}Ar.

Garnet from three samples from the P–L Unit was dated by Lu–Hf. One sample, for which we also obtained an ^{39}Ar–^{40}Ar age, was additionally dated by Sm–Nd (Electronic Appendix Table 3). The choice of a suitable cogenetic mineral having a low parent/daughter ratio is necessary to accurately estimate the isochron age. For Vaud003, a garnet–omphacite pair gave a Lu–Hf age of $59{\cdot}6 \pm 5{\cdot}2$ Ma and an indistinguishable Sm–Nd age of $45{\cdot}7 \pm 14{\cdot}2$ Ma. For Lan003, a garnet–glaucophane pair gave $54{\cdot}9 \pm 4{\cdot}3$ Ma. Both Vaud003 and Lan003 display a prograde HP assemblage. In contrast, Lev008 was extensively retrogressed in the upper greenschist facies; a garnet–epidote pair gave $41{\cdot}3 \pm 7{\cdot}1$ Ma, significantly younger than the two HP assemblages.

The garnet ages allow us to round off the chronology of the Alpine metamorphic cycle in the study area. Lu–Hf and Sm–Nd data are usually interpreted as dating prograde garnet growth prior to the eclogitic peak-*P* conditions. Our data show that the subduction of the P–L Unit (early D_1 *sensu* Bucher *et al.*, 2004) started *c.* 59 Ma ago. The late stage of D_1 is dated at 47–48 Ma by white mica grown syn-kinematically. Greenschist-facies conditions during exhumation (D_2) were reached between 43 and 39 Ma ago; this diachronism was caused by an east-to-west migration of deformation (Bucher *et al.*, 2004). Ages of *c.* 35 Ma are observed around the tectonic contact between the Ruitor and Zone Houillère Units, indicating deformation during a late stage of D_2 (Bucher *et al.*, 2004). Nappe refolding (D_3), not being associated with neoformed K-bearing minerals, could not be dated in the area of our study. The timing of D_3 is inferred from the regional context, which indicates that thrusting at the front of the Penninic units (Roselend Thrust; Loprieno *et al.*, 2011) in the western sector of the ECORS-CROP profile (Fig. 1) overlapped with the late stages of D_3 in our area. This thrust was dated at 34–30 Ma (Fügenschuh & Schmid,

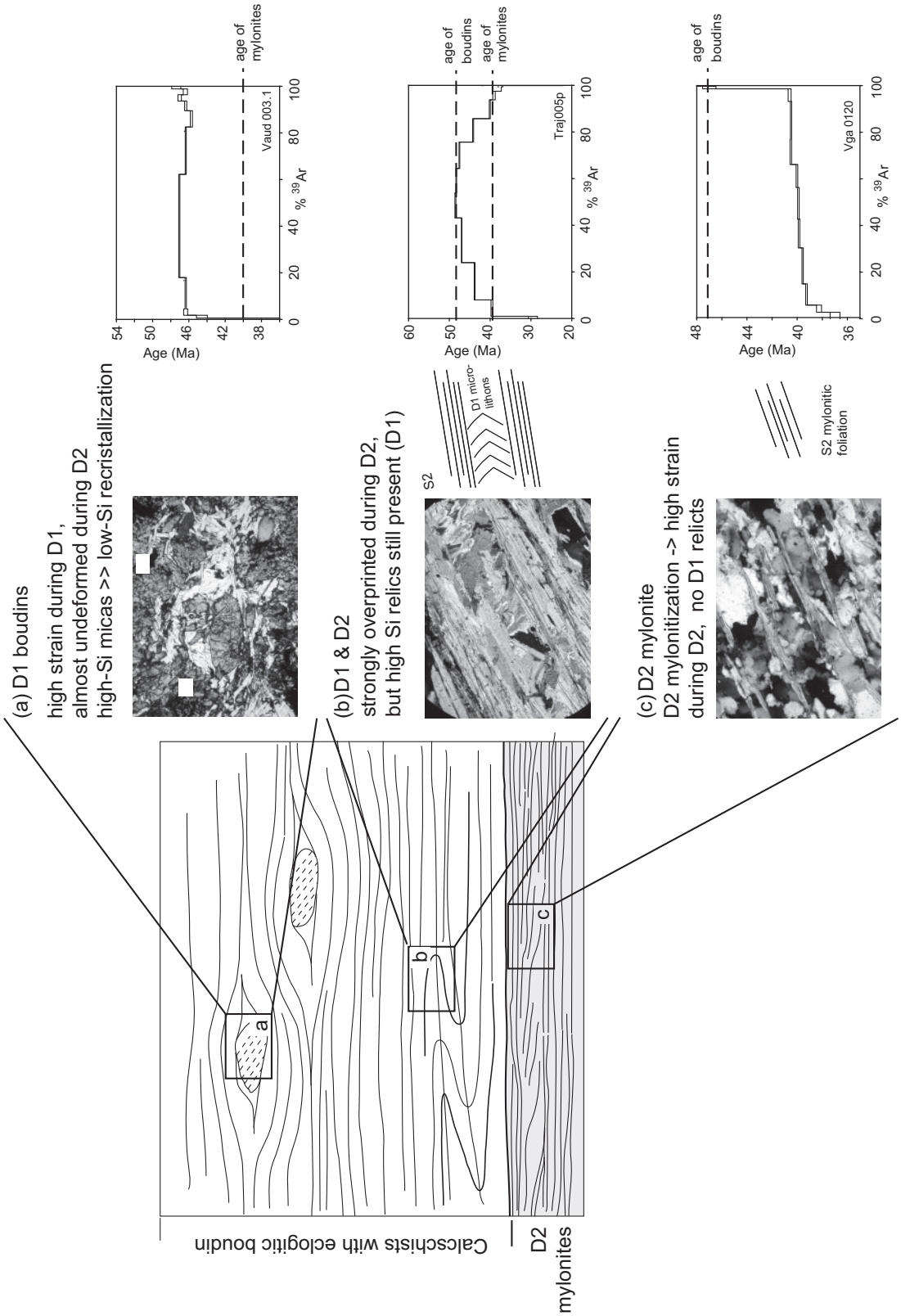

Fig. 14. Schematic compilation illustrating the major influence of deformation on the recorded ages. (a) Samples containing only D_1 mica (evidenced by microstructural and EMP analysis) show isochemical ages of 47 ± 1 Ma. (b) D_1 and D_2 mica, both present in the matrix of the boudins, yielding discordant age spectra typical for mixtures. (c) D_2 mylonites without D_1 relicts showing isochemical ages of 40 Ma.

2003; Simon-Labric *et al.*, 2009), which implies that D_3 probably took place sometime between 35 and 30 Ma, with local timing variations (Bucher *et al.*, 2004).

Comparison with literature

The literature on other sectors of the Western Alps provides time constraints on their tectono-metamorphic evolution that are easily harmonized with the petrological–geochronological framework proposed here. Dal Piaz *et al.* (2001) analysed white mica from metabasic eclogites in the most internal part of the P–L Unit by the ^{39}Ar–^{40}Ar incremental heating technique. Those researchers, not discussing Cl/K systematics, interpreted all their ages in the range between 41 and 46 Ma as representing HP formation ages, because Rb–Sr dating yielded the same age range. This interpretation has interesting implications. First, if one adopts the T_c approach, the statement of Dal Piaz *et al.* (2001) amounts to assigning a value for T_c to the K–Ar system that is not very different from that of the Rb–Sr system, and moreover, substantially above 500°C. Second, if the HP mineral ages are interpreted as formation ages, the possibility of obtaining mixed ages produced by the subsequent retrograde tectono-metamorphic evolution is very likely [albeit not mentioned by Dal Piaz *et al.* (2001)], because mica that was newly formed during the post-HP exhumation–retrogression must be retaining its Ar signature as well. For an equivalent of the P–L Unit, the Voltri Group eclogite (150 km SE of our study area), Federico *et al.* (2005) found ages around 49 Ma for eclogitic parageneses and ages <40 Ma for the retrogression. This suggests that the average age around 43 Ma reported by Dal Piaz *et al.* (2001) may record a mixture of eclogitic mica (with an age of *c.* 47 Ma, compatible with the HP age proposed here) and partially retrogressed micas younger than 41 Ma. The mafic rocks analysed by Dal Piaz *et al.* (2001), by analogy to sample Vaud003, date only the late stages during D_1.

White mica ^{39}Ar–^{40}Ar ages between 25 and 300 Ma were reported by Markley *et al.* (1998) for the Siviez–Mischabel nappe, which corresponds to the NE continuation of the Ruitor Unit of this study according to Gouffon (1993). Although their data do not show an age difference for different grain sizes (Markley *et al.*, 1998, pp. 420–421), those researchers proposed that diffusion controls the total gas K–Ar ages of white mica in the central Siviez–Mischabel nappe. Furthermore, Markley *et al.* stated that Hercynian mica is rimmed by 60 Ma old mica and concluded that these samples overestimate the timing of deformation by 20 Ma. Giorgis *et al.* (1999) reported pre-Alpine ages and proposed a Variscan P–T path from the ^{39}Ar–^{40}Ar data. Within our interpretative scheme, their staircase-shaped age spectra represent multiple mica generations and cannot be used to infer the ages of the pure D_1 or D_2 mica growth in the absence of petrological–chemical studies at the micrometre scale.

Chopin & Maluski (1980) reported discordant ^{39}Ar–^{40}Ar age spectra, interpreted as Cretaceous mica ages, from the Gran Paradiso Unit (a southwestern equivalent of the Monte Rosa nappe, both being parts of the most internal Briançonnais). It is likely that their samples, like some of the present study, record mixed ages between detrital and metamorphic mica generations.

Freeman *et al.* (1997) proposed an interpretation of the greenschist-facies evolution on the basis of Rb–Sr microsampling ages on white mica. They proposed 34 Ma as the age of back-thrusting along a shear zone (their Entrelor Shear Zone). However, we consider this shear zone as a refolded D_2 nappe contact rather than a back-thrust (Bucher *et al.*, 2003) because the stretching lineation used by Freeman *et al.* is related to a D_2 thrust that was overturned by D_3 back-folding (Bucher *et al.*, 2003; Bousquet, 2008).

In the Zone Houillère Unit, adjacent to the Houiller Front (Fig. 2) and the Valaisan domain (Fügenschuh *et al.*, 1999; Loprieno *et al.*, 2011), Freeman *et al.* (1998) reported Rb–Sr white mica ages for other samples from the same area. Even if, strictly speaking, their isochrons for detrital minerals do not rigorously meet the requirement that all phases be in equilibrium at time zero, most of their mica samples are sufficiently radiogenic that the calculated ages are not over-sensitive to the isotopic composition of the initial Sr. Freeman *et al.* obtained pre-Alpine ages varying from 324 ± 7 Ma close to the front of the Zone Houillère Unit to 188 ± 3 Ma towards more internal positions. Our sample Rui9978 (from an intermediate position with respect to the regional distribution of their samples) confirms this trend, which further supports evidence for a mixture between metamorphic and detrital populations. This trend is also compatible with the observation that intensity of deformation and metamorphic temperature increase towards the SE (Fig. 2; Bucher *et al.*, 2003, 2004). Both Rui9978 and the samples of Freeman *et al.* (1998) are well below the T_c values of Jäger (1967) for the respective isotopic systems, and yet they underwent loss of radiogenic ^{40}Ar and ^{87}Sr. The fact that the Rb–Sr and K–Ar systems yield identical ages contradicts 'thermochronology', which does not predict any ^{87}Sr diffusion in white mica at such low temperatures. On the contrary, our data indicate that it is deformation-induced recrystallization, rather than diffusion, that is responsible for the exchange of both ^{40}Ar and ^{87}Sr, which are therefore expected to correlate (Villa *et al.*, 2006).

Reddy *et al.* (1999) concluded that Rb–Sr data for recrystallized white mica indicate that the Gressoney Shear Zone (GSZ), associated with top-to-the SE kinematics, was active between 45 and 36 Ma. Those researchers interpreted the GSZ as the upper boundary of an extrusion channel active during D_2 exhumation. In our study D_2 is interpreted to have been active between 43 and 35 Ma,

consistent with the study of Reddy *et al.* (2003), and with the dating at 39 Ma of the retrograde shearing during exhumation in the neighbouring Gran Paradiso Massif (Rosenbaum *et al.*, 2012).

Agard *et al.* (2002) dated white mica from the P–L Unit *c.* 60 km to the south of our sampling area. The ages that those workers proposed for the eclogitic and retrogressive metamorphic stages are similar to the results of our study. All along strike in the Western Alps arc, Cretaceous apparent mica ages were observed (Monte Rosa, Gran Paradiso, etc.; Agard *et al.*, 2002, fig. 3). Monié (1990) also observed ^{40}Ar inheritance in HP phengite. It seems likely that the observations made in the present study are not limited to our study area, but probably also hold true for corresponding units further north and south. Our work provides a straightforward explanation for the excessively high (60–130 Ma) ages recorded only by mica in most of the HP portions of the Alps. These Cretaceous apparent ages are due to relict pre-Alpine micas, which were incompletely degassed owing to a combined effect of low temperatures (<550°C) and incomplete neocrystallization. We also reach two important methodological conclusions that agree with the results of Agard *et al.* (2002): (1) we argue that the ^{39}Ar–^{40}Ar isotopic system in HP phengite normally records formation and/or deformation ages; (2) our incremental heating and their laser ablation data yield consistent results. The compatibility of the data presented by Agard *et al.* (2002) with our data, together with the consistency of our data throughout the tectonic units along the ECORS-CROP transect, reinforces the correspondence between microstructures and ^{39}Ar–^{40}Ar ages obtained for each sample. Those researchers also found consistency between ^{39}Ar–^{40}Ar mica age and relative age of the white mica as inferred from macro- and microstructural studies, and stated that this makes the hypothesis of 'excess ^{40}Ar' at the scale of the whole orogen very unlikely (Agard *et al.*, 2002, p. 612–613). Whereas the study of Agard *et al.* (2002) applies to the more internal P–L Unit, our study extends these findings to the more external Briançonnais paleogeographical domain. The Lu–Hf age of the epidote–garnet retrograde assemblage (41·3 ± 7·1 Ma, Lev008) further reduces the likelihood that excess ^{40}Ar had a major effect. In our study area, excess ^{40}Ar plays a negligible role compared with that of recrystallization and/or inheritance. Hence, we disagree with internally inconsistent criteria (e.g. Reddy *et al.*, 2003) to reject the age of some of the samples.

Other areas of the Western Alps can be constrained by the ^{39}Ar–^{40}Ar data of Agard *et al.* (2002) from an area further south, and by the Rb–Sr data for the GSZ of Reddy *et al.* (1999), to a similar time frame to that of the transect studied here. Underplating of the South Penninic suture zone by the Briançonnais units in Eastern Switzerland started at *c.* 50 Ma as indicated by Rb–Sr white mica ages (Bachmann *et al.*, 2009). This is consistent with the 47–48 Ma age for the eclogitic mica crystallization proposed here.

Agreement regarding the P–T evolution, the kinematics and the geochronological data between these studies indicates that the geodynamic model of Bucher *et al.* (2003) might be valid for larger parts of the Western Alps. Further detailed studies that combine field, petrological and geochronological analyses will be needed to improve our understanding of the timing of the Alpine orogeny.

In summary, a general pattern consisting of three key points can be recognized in all available white mica age data from the Western Alps, in combination with the Lu–Hf and Sm–Nd garnet ages: (1) excess ^{40}Ar is negligible, whereas inherited ^{40}Ar is abundant because Ar diffusion is very slow; (2) Ar is lost by temperature-independent mica recrystallization anywhere between 250 and 600°C; (3) monogenetically recrystallized, single-generation neoformed mica gives reliable constraints on D_1 and D_2 ages, consistent with those of mica samples having the same microstructural setting, the same homogeneous chemical composition, and the same petrogenetic significance.

Mounting evidence for the same three-point pattern is forthcoming from other HP terrains. From the Attic–Cycladic HP rocks, Bröcker *et al.* (2013) also found mixed mica generations with ubiquitous Ar inheritance; they further observed that Ar retention is ≥Sr retention. This reinforces our suggestion that, in the absence of recrystallization, ^{87}Sr and ^{40}Ar loss are both minor if T is <500°C.

Our three-point pattern has general implications for the mechanisms controlling K–Ar ages. Because the radiogenic ^{40}Ar recoils away from the mica interlayer site occupied by ^{40}K into the T–O–T framework (Hetherington & Villa, 2007), the limiting factor for its transport is the mobility of the structure-forming cations (Villa, 2010), which is also rate-limiting for ^{87}Sr transport. This explains the observations of similar ^{40}Ar and ^{87}Sr retention (Bröcker *et al.*, 2013). The low intrinsic mobility of ^{40}Ar and ^{87}Sr, however, needs to be reconciled with the observation that ^{40}Ar and ^{87}Sr loss occurs at 250–300°C in the Zone Houillère Unit (this study; Freeman *et al.*, 1998). The factors controlling recrystallization during HP retrogression have been explained in detail by Parra *et al.* (2002). White mica–chlorite pairs in retrogressed HP rocks from Tinos (Attic–Cycladic belt) exhibit compositional variability that stems from the achievement of equilibrium only at the local mm-scale. Crystallization of new grains was fast, freezing in different segments of the retrogressive P–T path; equilibrium assemblages were achieved by crystallizing new grains showing progressive composition changes, whereas diffusive re-equilibration of relict grains was negligible, so that mineral compositions did not readjust to the changing P–T conditions (Parra *et al.*, 2002, pp. 54–55). As

P–T conditions alone were evidently not sufficient to reset mineral compositions, it is necessary to take into account the presence of aqueous fluids (a_{H2O}), the availability of solutes (X), and the intensity of D, and to consider that the actual control on mineral compositions is a function of P, T, a_{H2O}, X and D. An aqueous fluid is always required, as it is 'the principal catalyst of metamorphic reactions' (Parra *et al.*, 2002, p. 54; Putnis, 2009), and therefore of isotope exchange (Villa, 2010). Strain focusing localizes deformation-enhanced reactions to a progressively smaller volume, leaving the rest of the rock unaffected; thus deformation vastly prevails over diffusion. As documented by Worley *et al.* (1997), diffusion is detectable only at T much higher than 520°C. This additional, independent argument rounds off the evidence reviewed here that Ar retention in white mica is nearly complete at $T < 500$°C as long as the mineral is not recrystallized.

The regional distribution of eastward decreasing mica ages (Fig. 3) could be mistaken for a temperature-dependent pattern amenable to thermochronology. To the extent that more deformed rocks also generally record a higher metamorphic grade, the younger samples in the east indeed also experienced higher temperatures. However, when examined in close detail, the east–west age gradient is neither smooth nor decreasing throughout the easternmost unit, as would be expected if temperature alone were controlling K–Ar ages in mica. Instead, the context of all the independent lines of evidence reviewed above forces us to a very different interpretation. Diffusion of Ar in white mica is extremely slow. In most or all samples it is overrun by recrystallization, which mainly depends on a_{H2O}, X and D, and only marginally on T. This dependence provides the required explanation for why the K–Ar ages of detrital mica were reset (in unison with Rb–Sr ages) at 250–300°C in the Zone Houillère Unit, but were not reset to zero at 600°C in the Monte Rosa samples.

CONCLUSIONS

The early phase of HP metamorphism in the P–L Unit is indicated by Lu–Hf and Sm–Nd ages of *c.* 50–60 Ma for prograde garnet growth. The age of the eclogitic peak is closely constrained by ^{39}Ar–^{40}Ar dating of white mica, which grew at 10–15 kbar during the final stages of D_1, at 47–48 Ma in all tectono-metamorphic units. Exhumation related to D_2 (Bucher *et al.*, 2003, 2004) took place diachronously around 40 Ma. The *P–T–t* evolution of D_1 and D_2 proposed here is compatible with data from the P–L Unit further south in the Western Alps (Agard *et al.*, 2002). The comparison between the ^{39}Ar–^{40}Ar laser ablation data of Agard *et al.* (2002) and the data of this study confirms that mixed populations are correctly unravelled with the chemical information provided by the ^{39}Ar–^{40}Ar incremental heating technique. The Cl/K vs age common denominator isotope correlation diagrams allow the identification of heterochemical mica generations and of their ages.

Consistency within fractions of the same sample, between samples within a given tectonic unit, and also along the entire studied sector of the ECORS-CROP transect requires that neither temperature-dependent diffusive loss of ^{40}Ar nor gain of excess ^{40}Ar played an important role in the case of our samples. The K–Ar isotopic record of all samples from the ECORS-CROP transect and the Monte Rosa nappe was mainly controlled by the following processes. (1) ^{40}Ar inheritance is observed in preserved petrographic pre-Alpine relicts that are mixed with Alpine mica populations, and in D_1 relicts that are mixed with a D_2 population. Inherited ^{40}Ar is retained even in relict grains subjected to metamorphic temperatures ≥500°C. In the only sample showing permissible evidence for ^{40}Ar diffusion, the inferred diffusion parameters ($E = 250$ kJ mol^{-1}, $D'_0 < 0{\cdot}03$ cm^2 s^{-1}) confirm that diffusion is a very slow and hence very inefficient way to reset K–Ar ages. (2) ^{40}Ar loss from mica occurs instead by temperature-independent, deformation-induced and fluid-assisted recrystallization between 250 and 600°C. (3) ^{39}Ar–^{40}Ar stepwise heating data with a chemically homogeneous signature and a uniform age are observed only in samples containing mica of a single generation (D_1 or D_2), which are often highly deformed. This contrasts with samples where grain-scale microstructural and chemical observations indicate incomplete recrystallization and preservation of multiple populations, which are always the cause of staircase-shaped and/or upward-convex age spectra. In weakly deformed and poorly recrystallized samples the mass fraction of inherited grains is very high. The successful recognition of mixtures as a prerequisite for their reliable dating underscores that microstructural, microchemical and petrological analyses must not be viewed as optional 'accessory information', because they are as essential for any geochronological interpretation as the mass spectrometric analyses.

ACKNOWLEDGEMENTS

We thank all our colleagues from the 'Groupe Briançonnais', as well as Rainer Abart, Annett Büttner, Stefano Ceriani, Christian de Capitani, Martin Engi, Alexandra Heri, Lukas Keller, Jan Kramers and Marco Malusà for stimulating discussions. Mica samples Mrlk1 and Mrlk3 were separated and provided by Lukas Keller. Reviews by R. Schuster and W. Müller on an earlier version of this paper, as well as those by J. Glodny, M. Flowerdew and an anonymous reviewer, helped to improve the presentation. The editorial handling by R. Gieré was especially constructive.

FUNDING

The Swiss National Science Foundation provided support for this work through grant 20-63391.00 to S.M.S.

SUPPLEMENTARY DATA

Supplementary data for this paper are available at *Journal of Petrology* online.

REFERENCES

Agard, P., Monié, P., Jolivet, L. & Goffé, B. (2002). Exhumation of the Schistes Lustrés complex: *in situ* laser probe $^{40}Ar/^{39}Ar$ constraints and implications for the Western Alps. *Journal of Metamorphic Geology* **20**, 599–618.

Allaz, J., Berger, A., Engi, M. & Villa, I. M. (2011). The effects of retrograde reactions and of diffusion on ^{39}Ar–^{40}Ar ages of micas. *Journal of Petrology* **52**, 691–716.

Amstuz, A. (1955). Rocher du ravin de Lessert dans la Val D'Aoste. *Archives des Sciences de Genève* **8**, 6–9.

Amstuz, A. (1962). Notice pour une carte géologique de la Vallée de Cogne et de quelques autres espaces au Sud d'Aoste. *Archives des Sciences de Genève* **15**, 1–104.

Bachmann, R., Glodny, J., Oncken, O. & Seifert, W. (2009). Abandonment of the South-Penninic–Austroalpine paleosubduction zone, Central Alps, and shift from subduction erosion to accretion: constraints from Rb/Sr geochronology. *Journal of the Geological Society, London* **166**, 217–231.

Ballèvre, M. & Merle, O. (1993). The Combin Fault: compressional reactivation of a Late Cretaceous–Early Tertiary detachment fault in the Western Alps. *Schweizerische Mineralogische und Petrographische Mitteilungen* **73**, 205–227.

Baudin, T. (1987). Étude géologique du Massif du Ruitor (Alpes franco-italiennes): évolution structurale d'un socle briançonnais. PhD thesis, Université de Grenoble, 243 pp.

Belluso, E., Ruffini, R., Schaller, M. & Villa, I. M. (2000). Electron-microscope and Ar characterization of chemically heterogeneous amphiboles from the Palala Shear Zone, Limpopo Belt, South Africa. *European Journal of Mineralogy* **12**, 45–62.

Bertrand, J. M., Pidgeon, R. T., Leterrier, J., Gouillot, F., Gasquet, D. & Gattiglio, M. (2000). SHRIMP and IDTIMS U–Pb zircon ages of the pre-Alpine basement in the Internal Western Alps (Savoy and Piemont). *Schweizerische Mineralogische und Petrographische Mitteilungen* **80**, 225–248.

Bocquet, J. (1974*a*). Le socle briançonnais de Vanoise (Savoie): arguments en faveur de son âge anté-alpin et de son polymétamorphisme. *Comptes Rendus de l'Académie des Sciences* **278**, 2601–2604.

Bocquet, J. (1974*b*). Études minéralogiques et pétrographiques sur les métamorphismes d'âge alpin dans les Alpes françaises. PhD thesis, Université de Grenoble, 490 pp.

Bousquet, R. (2008). Metamorphic heterogeneities within a single HP unit: Overprint effect or metamorphic mix? *Lithos* **103**, 46–69.

Bousquet, R., Oberhänsli, R., Goffé, B., Jolivet, L. & Vidal, O. (1998). High-pressure–low-temperature metamorphism and deformation in the Bündnerschiefer of the Engadine window: implications for the regional evolution of the eastern Central Alps. *Journal of Metamorphic Geology* **16**, 657–674.

Bousquet, R., Goffé, B., Vidal, O., Oberhänsli, R. & Patriat, M. (2002). The tectono-metamorphic history of the Valaisan domain from the Western to the Central Alps: New constraints on the evolution of the Alps. *Geological Society of America Bulletin* **114**, 207–225.

Bröcker, M., Baldwin, S. & Arkudas, R. (2013). The geological significance of $^{40}Ar/^{39}Ar$ and Rb–Sr white mica ages from Syros and Sifnos, Greece: a record of continuous (re)crystallization during exhumation? *Journal of Metamorphic Geology* **31**, 629–646.

Bucher, S. (2003). The Briançonnais units along the ECORS-CROP transect (Italian–French Alps): structures, metamorphism and geochronology. PhD thesis, Universität Basel, 175 pp.

Bucher, S. & Bousquet, R. (2007). Metamorphic evolution of the Briançonnais units along the ECORS-CROP profile (Western Alps): New data on metasedimentary rocks. *Swiss Journal of Geosciences* **100**, 227–242.

Bucher, S., Schmid, S. M., Bousquet, R. & Fügenschuh, B. (2003). Late-stage deformation in a collisional orogen (Western Alps): nappe refolding, back-thrusting or normal faulting? *Terra Nova* **15**, 109–117.

Bucher, S., Ulardic, C., Bousquet, R., Ceriani, S., Fügenschuh, B., Gouffon, Y. & Schmid, S. M. (2004). Tectonic evolution of the Briançonnais units along a transect (ECORS-CROP) through the Western Alps. *Eclogae Geologicae Helvetiae* **97**, 321–346.

Caby, R. (1996). Low-angle extrusion of high-pressure rocks and the balance between outward and inward displacements of Middle Penninic units in the Western Alps. *Eclogae Geologicae Helvetiae* **89**, 229–267.

Ceriani, S. & Schmid, S. M. (2004). From N–S collision to WNW-directed post-collisional thrusting and folding: Structural study of the Frontal Penninic Units in Savoie (Western Alps, France). *Eclogae Geologicae Helvetiae* **97**, 347–369.

Ceriani, S., Fügenschuh, B. & Schmid, S. M. (2001). Late-stage thrusting at the 'Penninic Front' in the Western Alps between Mont Blanc and Pelvoux massifs. *International Journal of Earth Sciences* **90**, 685–702.

Challandes, N., Marquer, M. & Villa, I. M. (2003). Dating the evolution of C–S microstructures: a combined $^{40}Ar/^{39}Ar$ and UV laserprobe analysis of the Alpine Roffna shear zone. *Chemical Geology* **197**, 3–19.

Chopin, C. & Maluski, H. (1980). ^{40}Ar–^{39}Ar dating of high pressure metamorphic micas from the Gran Paradiso area (Western Alps): evidence against the blocking temperature. *Contributions to Mineralogy and Petrology* **74**, 109–122.

Chopin, C. & Monié, P. (1984). A unique magnesiochloritoid-bearing, high-pressure assemblage from the Monte Rosa, Western Alps: petrologic and ^{40}Ar–^{39}Ar radiometric study. *Contributions to Mineralogy and Petrology* **87**, 388–398.

Cigolini, C. (1995). Geology of the Internal Zone of the Grand Saint Bernard Nappe: a metamorphic Late Paleozoic volcano-sedimentary sequence in South-Western Aosta Valley (Western Alps). In: Lombardo, B. (ed.) *Studies on Metamorphic Rocks and Minerals of the Western Alps. A Volume in Memory of Ugo Pognante. Bollettino del Museo Regionale di Scienze Naturali Torino (Supplemento)* **13**, 293–328.

Cole, D. R., Ohmoto, H. & Lasaga, A. C. (1983). Isotopic exchange in mineral–fluid systems. I. Theoretical evaluation of oxygen isotopic exchange accompanying surface reactions and diffusion. *Geochimica et Cosmochimica Acta* **47**, 1681–1693.

Dahl, P. S. (1996*a*). The effects of composition on retentivity of Ar and O in hornblende and related amphiboles: a field-tested empirical model. *Geochimica et Cosmochimica Acta* **60**, 3687–3700.

Dahl, P. S. (1996*b*). The crystal-chemical basis for Ar retention in micas: inferences from interlayer partitioning and implications for geochronology. *Contributions to Mineralogy and Petrology* **123**, 22–39.

Dal Piaz, G. V. (1999). The Austroalpine–Piedmont nappe stack and the puzzle of alpine Tethys. *Memorie di Scienze Geologiche* **51**, 155–176.

Dal Piaz, G. V., Cortiana, G., Del Moro, A., Martin, S., Pennacchioni, G. & Tartarotti, P. (2001). Tertiary age and

paleostructural inferences of the eclogitic imprint in the Austroalpine outliers and Zermatt–Saas ophiolite, western Alps. *International Journal of Earth Sciences* **90**, 668–684.

De Sigoyer, J., Chavagnac, V., Blichert-Toft, J., Villa, I. M., Luais, B., Guillot, S., Cosca, M. A. & Mascle, G. (2000). Dating the Indian continental subduction and collisional thickening in the northwest Himalaya: Multichronology of the Tso Morari eclogites. *Geology* **28**, 487–490.

Dewey, J. F., Helman, M. L., Turco, E., Hutton, D. H. W. & Knott, S. D. (1989). Kinematics of the western Mediterranean. In: Coward, M. P., Dietrich, D. & Park, R. G. (eds) *Alpine Tectonics. Geological Society, London, Special Publications* **45**, 265–283.

Di Vincenzo, G., Ghiribelli, B., Giorgetti, G. & Palmeri, R. (2001). Evidence of a close link between petrology and isotope records; constraints from SEM, EMP, TEM and *in situ* ^{40}Ar–^{39}Ar laser analyses on multiple generations of white micas (Lanterman Range, Antarctica). *Earth and Planetary Science Letters* **192**, 389–405.

Di Vincenzo, G., Carosi, R. & Palmeri, R. (2004). The relationship between tectono-metamorphic evolution and argon isotope records in white mica: constraints from *in situ* ^{40}Ar–^{39}Ar laser analysis of the Variscan basement. *Journal of Petrology* **45**, 1013–1043.

Dodson, M. H. (1973). Closure temperature in cooling geochronological and petrological systems. *Contributions to Mineralogy and Petrology* **40**, 259–274.

Droop, G. T. R., Lombardo, B. & Pognante, U. (1990). Formation and distribution of eclogite facies rocks in the Alps. In: Carswell, E. D. A. (ed.) *Eclogite Facies Rocks*. Glasgow: Blackie, pp. 225–259.

Ellenberger, F. (1958). *Étude géologique du pays de Vanoise. Mémoire du Service Géologique de France*, 561 p.

Elter, G. (1960). La zona pennidica dell'alta e media Val d'Aosta e le unità limitrofe. *Memorie dell'Istituto di Geologia dell'Università di Padova* **22**, 113.

Elter, G. (1972). Contribution à la connaissance du Briançonnais interne et de la bordure piémontaise dans les Alpes Graies nord-orientales et considérations sur les rapports entre les zones du Briançonnais et des Schistes Lustrés. *Memorie dell'Istituto di Geologia dell'Università di Padova* **28**, 1–19.

Engi, M., Scherrer, N. & Burri, T. (2001). Metamorphic evolution of pelitic rocks of the Monte Rosa Nappe; constraints from petrology and single grain monazite age data. *Schweizerische Mineralogische und Petrographische Mitteilungen* **81**, 305–328.

Fabre, J. (1961). *Contribution à l'étude de la Zone Houillère Briançonnais en Maurienne et en Tarentaise (Alpes Savoie). Mémoires du Bureau de Recherches Géologiques et Minières* **2**, 315 p.

Federico, L., Capponi, G., Crispini, L., Scambelluri, M. & Villa, I. M. (2005). ^{39}Ar/^{40}Ar dating of high-pressure rocks from the Ligurian Alps: evidence for a continuous subduction–exhumation cycle. *Earth and Planetary Science Letters* **240**, 668–680.

Feys, R. (1963). *Étude géologique du Carbonifère briançonnais (Hautes-Alpes). Mémoires du Bureau de Recherches Géologiques et Minières* **6**, 387 p.

Foland, K. A. (1979). Limited mobility of argon in metamorphic terrains. *Geochimica et Cosmochimica Acta* **43**, 793–801.

Foland, K. A. (1983). ^{40}Ar/^{39}Ar incremental heating plateaus for biotites with excess Ar. *Chemical Geology* **41**, 3–21.

Freeman, S. R., Inger, S., Butler, R. W. H. & Cliff, R. A. (1997). Dating deformation using Rb–Sr in white mica: Greenschist facies deformation ages from the Entrelor shear zone, Italian Alps. *Tectonics* **16**, 57–76.

Freeman, S. R., Butler, R. W. H., Cliff, R. A., Inger, S. & Barnicoat, A. C. (1998). Deformation migration in an orogen-scale shear zone array: an example from the Basal Briançonnais Thrust, internal Franco-Italian Alps. *Geological Magazine* **135**, 349–367.

Frezzotti, M. L., Cesare, B. & Scambelluri, M. (2004). Fluids at extreme *P–T* metamorphic conditions: the message from high-grade rocks. *Periodico di Mineralogia* **73**,Special Issue 2, 209–219.

Fügenschuh, B. & Schmid, S. M. (2003). Late stages of deformation and exhumation of an orogen constrained by fission-track data: a case study in the Western Alps. *Geological Society of America Bulletin* **115**, 1425–1440.

Fügenschuh, B., Loprieno, A., Ceriani, S. & Schmid, S. (1999). Structural analysis of the Subbriançonnais and Valais units in the area of Moûtiers (Savoy, Western Alps): paleogeographic and tectonic consequences. *International Journal of Earth Sciences* **88**, 201–218.

Giletti, B. J. (1974). Studies in diffusion I: argon in phlogopite mica. In: Hofmann, A. W., Giletti, B. J., Yoder, H. S. & Yund, R. A. (eds) *Geochemical Transport and Kinetics. Carnegie Institution of Washington Publication* **634**, 107–115.

Giorgis, D., Thélin, P., Stampfli, G. M. & Bussy, F. (1999). The Mont-Mort metapelites: Variscan metamorphism and geodynamic context (Briançonnais basement, Western Alps, Switzerland). *Schweizerische Mineralogische und Petrographische Mitteilungen* **79**, 381–398.

Gouffon, Y. (1993). *Géologie de la 'nappe' du Grand St-Bernard entre la Doire Baltée et la frontière suisse (Vallée d'Aoste—Italie). Mémories de Géologie (Lausanne)* **12**, 147 p.

Graham, C. M. (1981). Experimental hydrogen isotope studies III: Diffusion of hydrogen in hydrous minerals, and stable isotope exchange in metamorphic rocks. *Contributions to Mineralogy and Petrology* **76**, 216–228.

Gréber, C. (1965). *Flore et stratigraphie du Carbonifère des Alpes françaises. Mémoires du Bureau de Recherches Géologiques et Minières* **21**, 380 p.

Hames, W. E. & Cheney, J. T. (1997). On the loss of ^{40}Ar* from muscovite during polymetamophism. *Geochimica et Cosmochimica Acta* **61**, 3863–3872.

Hammerschmidt, K. & Frank, E. (1991). Relics of high pressure metamorphism in the Lepontine Alps (Switzerland)—^{40}Ar/^{39}Ar and microprobe analyses on white K-micas. *Schweizerische Mineralogische und Petrographische Mitteilungen* **71**, 261–274.

Harrison, T. M., Célérier, J., Aikman, A. B., Hermann, J. & Heizler, M. T. (2009). Diffusion of ^{40}Ar in muscovite. *Geochimica et Cosmochimica Acta* **73**, 1039–1051.

Heri, A. R., Robyr, M. & Villa, I. M. (2013). Petrology and geochronology of the 'muscovite standard' B4M. In: Jourdan, F., Mark, D. & Verati, C. (eds) *^{40}Ar/^{39}Ar Dating: from Geochronology to Thermochronology, from Archaeology to Planetary Sciences. Geological Society, London, Special Publications* **378**, 69–78.

Hess, J. C., Lippolt, H. J. & Wirth, R. (1987). Interpretation of ^{40}Ar/^{39}Ar spectra of biotites—evidence from hydrothermal degassing experiments and TEM studies. *Chemical Geology* **66**, 137–149.

Hetherington, C. J. & Villa, I. M. (2007). Barium silicates of the Berisal Complex, Switzerland: A study in geochronology and rare-gas release systematics. *Geochimica et Cosmochimica Acta* **71**, 3336–3347.

Hodges, K. V., Hames, W. E. & Bowring, S. A. (1994). ^{40}Ar/^{39}Ar age gradients in micas from a high-temperature–low-pressure metamorphic terrain; evidence for very slow cooling and implications for the interpretation of age spectra. *Geology* **22**, 55–58.

Jäger, E. (1967). Kritische Betrachtungen zur Interpretation der Alterswerte. In: Jäger, E., Niggli, E. & Wenk, E. (eds) *Altersbestimmungen an Glimmern in den Zentralalpen. Beiträge zur Geologischen Karte, Neue Folge* **134**, 38–40.

Keller, L. M., Abart, R., Stünitz, H. & De Capitani, C. (2004). Deformation, mass transfer and reactions in an eclogite facies shear zone in a polymetamorphic metapelite (Monte Rosa, Western Alps). *Journal of Metamorphic Geology* **22**, 97–118.

Keller, L. M., Hess, M., Fügenschuh, B. & Schmid, S. M. (2005). Structural and metamorphic evolution of the Camughera–Moncucco, Antrona and Monte Rosa units southwest of the Simplon line, Western Alps. *Eclogae Geologicae Helvetiae* **98**, 19–49.

Kelley, S. P. (2002). Excess argon in K–Ar and Ar–Ar geochronology. *Chemical Geology* **188**, 1–22.

Kleinhanns, I. C., Kreissig, K., Kamber, B. S., Meisel, T., Nägler, T. F. & Kramers, J. D. (2002). Combined chemical separation of Lu, Hf, Sm, Nd and REEs from a single rock digest: precise and accurate isotope determinations of Lu–Hf and Sm–Nd using multicollector-ICPMS. *Analytical Chemistry* **74**, 67–73.

Kuiper, K. F., Deino, A., Hilgen, F. J., Krijgsman, W., Renne, P. R. & Wijbrans, J. R. (2008). Synchronizing the rock clocks of Earth History. *Science* **320**, 500–504.

Lanphere, M. A. & Dalrymple, G. B. (1976). Identification of excess ^{40}Ar by the ^{40}Ar/^{39}Ar age spectrum technique. *Earth and Planetary Science Letters* **32**, 141–148.

Lasaga, A. C. (1986). Metamorphic reaction rate laws and development of isograds. *Mineralogical Magazine* **50**, 359–373.

Livi, K. J. T. & Abad, I. (2013). The role of transmission electron microscopy in the study of micas and related minerals in selected metamorphic environments. In: Nieto, F. & Livi, K. J. T. (eds) *Minerals at the Nanoscale. EMU Notes in Mineralogy* **14**, 217–259.

Loprieno, A., Bousquet, R., Bucher, S., Ceriani, S., Dalla Torre, F. H., Fügenschuh, B. & Schmid, S. M. (2011). The Valais units in Savoy (France): a key area for understanding the palaeogeography and the tectonic evolution of the Western Alps. *International Journal of Earth Sciences* **100**, 963–992.

Lugmair, G. W. & Marti, K. (1978). Lunar initial ^{143}Nd/^{144}Nd: Differential evolution of the lunar crust and mantle. *Earth and Planetary Science Letters* **39**, 349–357.

Malusà, M. G., Polino, R. & Martin, S. (2005). The Gran San Bernardo nappe in the Aosta valley (western Alps): a composite stack of distinct continental crust units. *Bulletin de la Société Géologique de France* **176**, 417–431.

Malusà, M. G., Polino, R. & Zattin, M. (2009). Strain partitioning in the axial NW Alps since the Oligocene. *Tectonics* **28**, TC3005.

Malusà, M. G., Faccenna, C., Garzanti, E. & Polino, R. (2011). Divergence in subduction zones and exhumation of high pressure rocks (Eocene Western Alps). *Earth and Planetary Science Letters* **310**, 21–32.

Markley, M. J., Teyssier, C., Cosca, M. A., Caby, R., Hunziker, J. C. & Sartori, M. (1998). Alpine deformation and ^{40}Ar/^{39}Ar geochronology of synkinematic white mica in the Siviez–Mischabel Nappe, western Pennine Alps, Switzerland. *Tectonics* **17**, 407–425.

Massonne, H.-J. & Schreyer, W. (1987). Phengite geobarometry based on the limiting assemblage with K-feldspar, phlogopite, and quartz. *Contributions to Mineralogy and Petrology* **96**, 212–224.

Mercier, D. & Beaudoin, B. (1987). Révision du Carbonifère Briançonnais: Stratigraphie et évolution du bassin. *Géologie Alpine* **13**, 25–31.

Monié, P. (1985). La méthode ^{39}Ar–^{40}Ar appliquée au metamorphism alpin dans le massif du Mont-Rose (Alpes Occidentales). Chronologie détaillée depuis 110 Ma. *Eclogae Geologicae Helvetiae* **78**, 487–516.

Monié, P. (1990). Preservation of Hercynian ^{40}Ar/^{39}Ar ages through high-pressure low-temperature Alpine metamorphism in the Western Alps. *European Journal of Mineralogy* **2**, 343–361.

Müller, W. (2003). Strengthening the link between geochronology, textures and petrology. *Earth and Planetary Science Letters* **206**, 237–251.

Müller, W., Kelley, S. P. & Villa, I. M. (2002). Dating fault-generated pseudotachylytes: comparison of ^{40}Ar/^{39}Ar stepwise-heating, laser ablation and Rb–Sr microsampling analyses. *Contributions to Mineralogy and Petrology* **144**, 57–77.

Nazzareni, S., Comodi, P., Bindi, L., Safonov, O. G., Litvin, Yu. A. & Perchuk, L. L. (2008). Synthetic hypersilicic Cl-bearing mica in the phlogopite–celadonite join: A multimethodical characterization of the missing link between di- and tri-octahedral micas at high pressures. *American Mineralogist* **93**, 1429–1436.

Parra, T., Vidal, O. & Jolivet, L. (2002). Relation between the intensity of deformation and retrogression in blueschist metapelites of Tinos Island (Greece) evidenced by chlorite–mica local equilibria. *Lithos* **63**, 41–66.

Philippot, P., Blichert-Toft, J., Perchuk, A., Costa, S. & Gerasimov, V. (2001). Lu–Hf and Ar–Ar chronometry supports extreme rate of subduction zone metamorphism deduced from geospeedometry. *Tectonophysics* **342**, 22–38.

Purdy, J. W. & Jäger, E. (1976). K–Ar ages on rock-forming minerals from the Central Alps. *Memorie dell'Istituto di Geologia dell'Università di Padova* **30**, 1–32.

Putnis, A. (2009). Mineral replacement reactions. In: Oelkers, E. H. & Schott, J. (eds) *Thermodynamics and Kinetics of Water–Rock Interaction. Mineralogical Society of America and Geochemical Society, Reviews in Mineralogy and Geochemistry* **70**, 689–708.

Reddy, S. M., Wheeler, J. & Cliff, R. A. (1999). The geometry and timing of orogenic extension: an example from the Western Italian Alps. *Journal of Metamorphic Geology* **17**, 573–589.

Reddy, S. M., Wheeler, J., Butler, R. W. H., Cliff, R. A., Freeman, S., Inger, S., Pickles, C. & Kelley, S. P. (2003). Kinematic reworking and exhumation within the convergent Alpine Orogen. *Tectonophysics* **365**, 77–102.

Rex, D. C., Guise, P. G. & Wartho, J. A. (1993). Disturbed ^{40}Ar/^{39}Ar spectra from hornblendes: Thermal loss or contamination? *Chemical Geology* **103**, 271–281.

Rosenbaum, G., Menegon, L., Glodny, J., Vasconcelos, P., Ring, U., Massironi, M., Thiede, D. & Nasipuri, P. (2012). Dating deformation in the Gran Paradiso Massif (NW Italian Alps): Implications for the exhumation of high-pressure rocks in a collisional belt. *Lithos* **144**, 130–144.

Roure, F., Bergerat, F., Damotte, B., Mugnier, J.-L. & Polino, R. (1996). The ECORS-CROP Alpine seismic traverse. *Mémoires de la Société Géologique de France* **170**, 113 p.

Scherer, E. E., Münker, C. & Mezger, K. (2001). Calibration of the lutetium–hafnium clock. *Science* **293**, 683–686.

Schmid, S. M. & Kissling, E. (2000). The arc of the Western Alps in the light of new data on deep crustal structure. *Tectonics* **19**, 62–85.

Schmid, S. M., Fügenschuh, B., Kissling, E. & Schuster, R. (2004). Tectonic map and overall architecture of the Alpine orogen. *Eclogae Geologicae Helvetiae* **97**, 93–117.

Simon-Labric, T., Rolland, Y., Dumont, T., Heymes, T., Authemayou, C., Corsini, M. & Fornari, M. (2009). ^{40}Ar/^{39}Ar dating of Penninic front displacement (W Alps) during the Lower Oligocene (31–34 Ma). *Terra Nova* **21**, 127–136.

Steiger, R. H. & Jäger, E. (1977). Subcommission on Geochronology: Convention on the use of decay constants in geo- and cosmochronology. *Earth and Planetary Science Letters* **36**, 359–362.

Trümpy, R. (1966). Considérations générales sur le 'Verrucano' des Alpes Suisses. *Atti Società Toscana Scienze Naturali, Volume Speciale del Simposium sul Verrucano, Pisa 1966*, 212–232.

Ulardic, C. (2001). Strukturgeologische und petrographische Untersuchungen im Valgrisenche (Briançonnais der italienischen Alpen). MSc thesis, Universität Freiburg, 100 pp.

Valente, A. & Borghi, A. (2000). Tectono-metamorphic evolution of the anthracite-bearing basin of La Thuile (External Briançonnais zone). *Géologie Alpine* **76**, 151–163.

Vance, D., Müller, W. & Villa, I. M. (2003). Geochronology: linking the isotopic record with petrology and textures—an introduction. In: Vance, D., Müller, W. & Villa, I. M. (eds) *Geochronology: Linking the Isotopic Record with Petrology and Textures. Geological Society, London, Special Publications* **220**, 1–24.

Villa, I. M. (1998). Isotopic closure. *Terra Nova* **10**, 42–47.

Villa, I. M. (2001). Radiogenic isotopes in fluid inclusions. *Lithos* **55**, 115–124.

Villa, I. M. (2006). From the nm to the Mm: isotopes, atomic-scale processes, and continent-scale tectonic models. *Lithos* **87**, 155–173.

Villa, I. M. (2010). Disequilibrium textures vs equilibrium modelling: geochronology at the crossroads. In: Spalla, M. I., Marotta, A. M. & Gosso, G. (eds) *Advances in Interpretation of Geological Processes. Geological Society, London, Special Publications* **332**, 1–15.

Villa, I. M. & Hanchar, J. M. (2013). K-feldspar hygrochronology. *Geochimica et Cosmochimica Acta* **101**, 24–33.

Villa, I. M. & Puxeddu, M. (1994). Geochronology of the Larderello geothermal field; new data and the 'closure temperature' issue. *Contributions to Mineralogy and Petrology* **115**, 415–426.

Villa, I. M. & Williams, M. L. (2013). Geochronology of metasomatic events. In: Harlov, D. E. & Austrheim, H. (eds) *Metasomatism and the Chemical Transformation of Rock*. Berlin: Springer, pp. 171–202.

Villa, I. M., Grobéty, B., Kelley, S. P., Trigila, R. W. & Wieler, R. (1996). Assessing Ar transport paths and mechanisms in the McClure Mountains hornblende. *Contributions to Mineralogy and Petrology* **126**, 67–80.

Villa, I. M., Ruggieri, G. & Puxeddu, M. (1997). Petrological and geochronological discrimination of two white-mica generations in a granite cored from the Larderello–Travale geothermal field (Italy). *European Journal of Mineralogy* **9**, 563–568.

Villa, I. M., Hermann, J., Müntener, O. & Trommsdorff, V. (2000). ^{39}Ar–^{40}Ar dating of multiply zoned amphibole generations (Malenco, Italian Alps). *Contributions to Mineralogy and Petrology* **140**, 363–381.

Villa, I. M., Ruggieri, G., Puxeddu, M. & Bertini, G. (2006). Geochronology and isotope transport systematics in a subsurface granite from the Larderello–Travale geothermal system (Italy). *Journal of Volcanology and Geothermal Research* **152**, 20–50.

Warren, C. J., Kelley, S. P., Sherlock, S. C. & McDonald, C. S. (2012). Metamorphic rocks seek meaningful cooling rate: Interpreting ^{40}Ar/^{39}Ar ages in an exhumed ultra-high pressure terrane. *Lithos* **155**, 30–48.

Wartho, J. A. (1995). Apparent argon diffusive loss ^{40}Ar/^{39}Ar age spectra in amphiboles. *Earth and Planetary Science Letters* **134**, 393–407.

Wijbrans, J. R. & McDougall, I. (1986). ^{40}Ar/^{39}Ar dating of white micas from an Alpine high-pressure metamorphic belt on Naxos: the resetting of the argon isotopic system. *Contributions to Mineralogy and Petrology* **93**, 187–194.

Worley, B., Powell, R. & Wilson, C. J. L. (1997). Crenulation cleavage formation: Evolving diffusion, deformation and equilibration mechanisms with increasing metamorphic grade. *Journal of Structural Geology* **19**, 1121–1135.